UCLouvain

École polytechnique de Louvain

Simulation of real-time decision making for dose delivery in proton therapy

Author : **Estelle Loÿen**
Supervisors : **Benoît Macq**, **Damien Dasnoy-Sumell**
Readers : **Christophe De Vleeschouwer**, **Rudi Labarbe**, **Kevin Souris**
Academic year 2019–2020
Master [120] in Biomedical Engineering

Acknowledgements

The writing of this thesis was made possible thanks to several people who, through their advice and support, carried me through to the end.

First of all, I would like to thank my supervisor, Professor Benoît Macq, for agreeing to follow me in the development of this thesis. Thanks to him, I was able to put my knowledge to good use on a subject that has long fascinated me.

Next, I want to express my gratitude to Damien Dasnoy-Sumell for his enthusiasm for this subject and for his availability throughout the year, his help and advice without which the realization of this thesis would not have been possible.

I would also like to thank Kevin Souris, who has always taken the time to answer my questions. I thank him as well as Christophe De Vleeschouwer and Rudi Labarbe for agreeing to read this work.

Then I would like to thank my family, who during these five years of study have always believed in me. My mother, for the many hours spent helping me formulate and develop my ideas. My father, for the rereading of this dissertation. Martin, for taking the time to correct my English. Chloë for being there and for her advice. Finally, I would like to thank Louis for his constant support and encouragement.

Abstract

Nowadays, more than 10% of cancers are lung cancers. Radiotherapy is one of the methods used to treat this cancer. It uses radiation to irradiate the cancerous cells to kill them by blocking their ability to proliferate. Proton therapy is a particular radiotherapy technique that enables to deliver the dose locally at the level of the tumor. Proton therapy uses the Pencil Beam Scanning to deliver the dose by scanning point by point the tumor volume. However, the use of this technique leads to the phenomenon of interplay when used with a mobile tumor. If the movements of the PBS and of the tumor are not synchronized, the delivered dose within the target is not uniform and the surrounding tissue is also irradiated. Several methods have been studied to mitigate the effect of interplay. Some of those methods are used in routine while others are still in the research stage. In this context, we evaluate in this master thesis a new approach to reduce the effect of interplay. This new approach consists of a real-time decision making for dose delivery. This means that no treatment plan is fixed in advance and that the optimization of the position where to deliver the dose is done in real-time, taking into account the information received on the patient's anatomy and on the already delivered dose.

Contents

Acronyms

COGA COmpute GAin. 41

COGA_ONPODO COmpute GAin ONe POsition DOse. 41

COGA_TUCO COmpute GAin TUmor COnstraints. 42

COGA_TUVODO COmpute GAin TUmor VOlume DOse. 42

CT Computerized Tomography. 6

DNA DeoxyriboNucleic Acid. 1

DVH Dose-Volume Histogram. 9, 48

FIBESCMO FIxed BEam SCanning MOtion. 40

FITWSACO FIrst TWenty SAtisfying COnstraints. 40

GUI Graphical User Interface. vii, 35

HI Homogeneity Index. 56

MIACDO MInimum ACcumulated DOse. 41

MSE Mean Squared Error. 42

NSCLC Non-Small Cell Lung Cancer. 2

OAR Organ At Risk. 32

OS Optimized Sequence. 25

PBS Pencil Beam Scanning. 12

ROI Region Of Interest. 16

RS Regular Scanning. 25

SCLC Small Cell Lung Cancer. 2

WS Worst Sequence. 25

List of Figures

List of Tables

Chapter 1

Introduction

1.1 Medical background

Cancer is a pathology characterized by the presence of at least one malignant tumor which is created by the mutation of a normal cell. This mutation is caused by a genetic instability [1]. The cell's transformation can be due to a loss of cell cycle control, an insensitivity to apoptosis (cell suicide) or even due to abnormalities in the DNA repair. Actually, this transformation can be executed by many types of cells and this is the reason why there are different kinds of cancer, depending on the type of cells which are transformed [2]:

- **Lymphoma**: a cancer affecting the lymphatic cells, called the lymphocytes. In this case, the cancerous cells do not invade the blood flow, instead targeting the lymph nodes, increasing their sizes.
- **Carcinoma**: a tumor developed from epithelium's cells. This type of cancer is the most commonly diagnosed.
- **Sarcoma**: a tumor developed from cells of a conjunctive tissue. It can arise in bones, muscles, blood vessels, cartilages or other soft connective tissue.
- **Leukemia**: a blood cancer caused by the rise of white blood cells.

1.1.1 Cancer in figures

In 2018, around the world, 18.1 million people have been diagnosed with a cancer, of which 9.6 million died. Moreover, specialists feel that this number is going to increase every year because of three main factors: world population growth, global ageing and lifestyle degradation [3].

Let's take a closer look to the situation in Belgium, 68216 new cases of cancer have been registered in 2016. Among them, 99% of those diagnosed with a cancer are over 20 years old. For adults, 4 types of cancer represent more than 50% of all diagnosed cancers. Namely prostate cancer, breast cancer, lung cancer and colon cancer. While, in youngsters, the most frequent cancers are leukemia, lymphoma or brain tumors. Besides, of the 68216 new cases of 2016, 67% of diagnosed women were over 60 while 78% of men were of the same age group. This means that elderly are more frequently affected by cancer than younger people.

1.1.2 Lung cancer in particular

In this work, we mainly focus on mobile tumors, that's why we consider the lung cancer in particular. The lung cancer develops from bronchial cells. Actually, there are two different kinds of lung cancer depending on the origin of the bronchial cells causing the tumor [4]:

- **Small Cell Lung Cancer (SCLC)**: this kind of lung cancer represents about 15% of lung cancers. Although it is not the most frequent type of lung cancer, it is the most aggressive one. Small cells have the ability to metastasize many sites within the body very rapidly. This cancer is, therefore, discovered after the extensive spread of the metastasis. This kind of cancer is mainly due to smoking.
- **Non-Small Cell Lung Cancer (NSCLC)**: this kind of cancer represents about 85% of lung cancers. It is any type of epithelial lung cancer other than SCLC.

In Belgium, the number of those diagnosed with cancer rises each year and more than 8000 new cases of lung cancer are registered each year [5]. As you can observe on Fig.1.1a, this is more than 10% of the total number of cancers. Fig.1.1b shows that lung cancer is more diagnosed among men and, moreover, we know that most of them are over 60 [5].

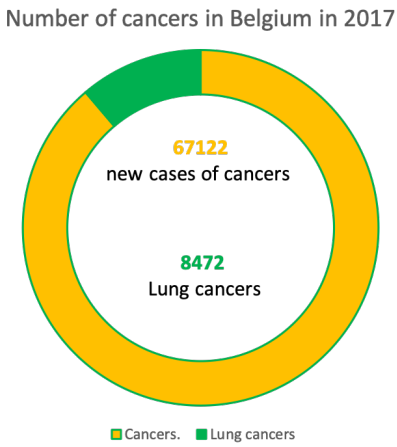

(a) Total number of new cases of cancers

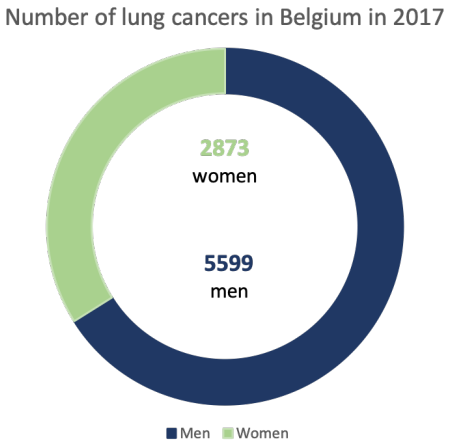

(b) Gender distribution of lung cancer

Figure 1.1: Belgian statistics for cancers and lung cancers in 2017, adapted from [5].

The choice of the treatment to cure this cancer depends on several factors: the patient's choice, the tumor's location, the kind of lung cancer and, finally, the stage of the disease. As you can see from Fig.1.2, there are 4 stages for lung cancer [6]:

- **Stage 1**: the diameter of the tumor is below three centimeters and the tumor is attached to the lung.
- **Stage 2**: the tumor reaches bronchi' lymph nodes.
- **Stage 3**: the tumor leads to metastasis in mediastinum's lymph nodes.
- **Stage 4**: the tumor spreads up to the other lung or others organs.

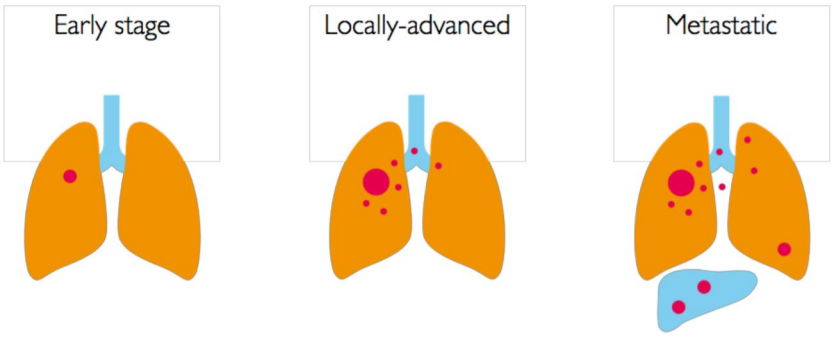

Figure 1.2: Different stages of lung cancer [7].

Three main treatments exist for lung cancer: chemotherapy, radiotherapy and surgery. They can be used alone or in combination [4].

Chemotherapy

This kind of treatment is used to treat non-small cells lung cancers. The chemotherapy consists of destroying cancerous cells by preventing their division and by eliminating them from the whole body. This kind of treatment is, usually, administered by an intravenous way. This technique can be used for all stages of the disease. But, depending on the stage of the cancer, this treatment will be prescribed alone or in combination with radiotherapy and/or surgery [8].

Radiotherapy

This kind of treatment is used to treat non-small cells lung cancers and small cells lung cancers. In the case of NSCLC, this method is generally employed for advanced diseases. But, it may also be prescribed in earlier stage of the disease when, for example, the surgery is impossible. In SCLC, radiotherapy is only used for localized forms of the cancer. The radiotherapy consists of irradiating the tumor in order to destroy it or to reduce its size. This kind of treatment is mostly administered for 5 consecutive days during 8 weeks [9]. This is the type of treatment we are working on, it will be explained in more detail in the next chapter.

Surgery

This kind of treatment is only used to treat NSCLC, and in an early stage of the disease. The surgery consists of removing a part of the lung, a lobe or even a whole lung. This depends on the localization of the tumor on the lung. In some cases, it may happen that the patient undergoes a chemotherapy before the surgery in order to reduce the tumor's size [10].

1.2 Objectives of this work

Currently, we find that the techniques used in the radiotherapy treatment of lung cancer are not optimal and this, in large part, due to the motion of the target occurring during the treatment. The dose delivery in radiotherapy must take into account this mobility but, nowadays, the treatment plan is developed at the beginning of the treatment during the optimization phase. In this case, the mobility of the lung is handled once and for all and the position of the tumor will not come up for review during the whole treatment.

The objective of this work is to try to control the tumor motion by a real-time decision making. In this situation, one has to determine in real-time if the dose must be delivered or not and this, in order to have a dose as uniform as possible in the tumor during the treatment. Moreover, the delivered dose must always satisfy the several constraints on the different organs. This real-time approach, if successful, will allow to suppress the treatment planning phase of the current clinical workflow of radiotherapy. Indeed, in this approach, the dose computation and the place to deliver it will be continuously reassessed to take into account the mobility of the lung, of the tumor and of the surrounding organs at risk.

1.3 Organization of the document

To ensure that the approach we have developed is the clearest and most intelligible possible, we decided to divide this work in three parts. We believe it is important to fully understand and master the characteristics of radiotherapy and proton therapy but also the differences between them. These will be discussed and developed in Chapter 2. As mentioned earlier in this work, the mobility of the target is the key but also the difficulty of the treatment. Chapter 3 will be devoted to the interplay phenomenon. We will define and explain it in detail and also the different methods that have already be studied to master it. However, these methods did not achieve the final objective and we will try to explain why. Understanding why an approach does not achieve satisfying results can push us to innovate in our approach. Once we have developed the principle of interplay, we will discuss our personal approach in Chapter 4. In what way it is different and innovative from the methods already used to reduce the effect of interplay and we will highlight the results we have obtained.

Chapter 2

Radiotherapy

As already said, radiotherapy is one of the techniques used to treat lung cancers. It is one of the leading methods to treat cancer and to improve patient's life quality. There are two kinds of radiation therapy: internal radiotherapy and external radiotherapy.

In the case of internal radiotherapy, also called brachytherapy, the radiation source is injected inside the body using a needle. The location can be next to or inside the tumor. This type of radiotherapy has a big advantage as it allows for an important quantity of delivered dose inside the tumor while keeping the dose delivered to the surrounding healthy tissue to a minimum [11].

The external radiotherapy is delivered from a machine outside the body. In this case, it is possible to have a high dose in the tumor and a small one outside by delivering beams from different angles [12]. This kind of radiotherapy is the most commonly used, prescribed 60% of the time. We will study this type of radiotherapy in detail before introducing proton therapy, a particular case of external radiotherapy that we use in our approach.

2.1 Basic mechanisms of radiotherapy

In this section of the work, the principles on which radiotherapy is based will be highlighted. The purpose of radiotherapy is to eradicate the tumor, this means to kill all the cancerous cells using the radiation beam while preserving the surrounding tissue safe.

2.1.1 Ionizing radiation

The basic principle of radiotherapy is ionizing radiation. It uses high-energy particles or waves to destroy or damage cancerous cells. These particles can be X-rays, gamma rays, electrons beam or protons beam [13]. The penetrating power of ionizing radiation is the main characteristic taken into account to determine the application of this ionizing radiation in radiotherapy. The deeper the tumor within a patient, the higher the penetrating power required of the radiation. Then, the radiation will be able to kill the exposed cells. Radiation blocks the ability of cells to divide and proliferate by damaging their genetic material [7].

2.1.2 Dose sculpting

As the main goal of radiotherapy is to damage the tumor while sparing the surrounding tissue, it is important to modulate the beam intensity according to the direction in which it arrives in order to have a higher dose in the tumor than in the surrounding organs. This process is called dose sculpting. The beam can be delivered from different directions thanks to a gantry rotating around the patient and dose sculpting is performed using a multi-leaf collimator placed on this gantry. There are two main ways to perform dose sculpting [7].

- **Conventional conformation**: this technique of dose sculpting uses a Computerized Tomography (CT) scanner to get images that will let us reconstruct a three-dimensional target volume. This technique allows a better spatial distribution of the dose but, it is unable to exclude the normal tissue around the tumor. As shown in Fig.2.1(left), in order to cover the whole volume of the tumor, the beam is delivered from three different directions. Moreover, the radiation intensity is the same for all beamlets in the beam resulting in the dose being delivered in the tumor, but also in surrounding organs at risk [14].
- **Intensity modulation**: this technique is an improvement of the previous one. For the case of the tumor on Fig.2.1, this technique is very useful as it spares the surrounding healthy tissue. As represented in Fig.2.1(right), in this technique, the beam is composed of hundreds of beamlets which have all a different radiation intensity. This variation of radiation intensity enables a very complex pattern reconstruction and a precise target shaping. With this technique, it is possible to spare the healthy surrounding tissue while the tumor shape is concave [14].

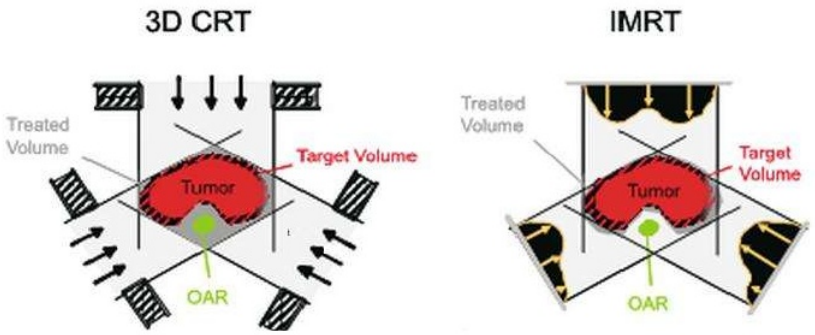

Figure 2.1: Two main ways to perform dose sculpting : (left) conventional conformation versus (right) intensity modulation [7]. This makes it possible to have a higher dose in the tumor than in the surrounding tissue.

2.1.3 Radiobiology

As already said, the purpose of radiotherapy is to damage cancerous cells, or better to kill them, by delivering sufficient dose of ionising radiation in this target area. Radiobiology is based on four principles [15]:

- **Redistribution**: cells can survive to irradiation because they were blocked in a resistant phase of cell cycle, then redistribute into more sensitive phases during subsequent dose of radiation.

- **Reoxygenation**: cells can be resistant to irradiation due to hypoxia, they become more radiosensitive when they are reoxygenated.
- **Repair**: cells can be repaired by an enzymatic process after a damage to their strands of DNA.
- **Repopulation**: cells are able to repopulate or regenerate themselves after being injured.

2.2 Clinical Workflow

In this section, the different steps of the radiotherapy process will be explained. This clinical workflow is represented on Fig.2.2.

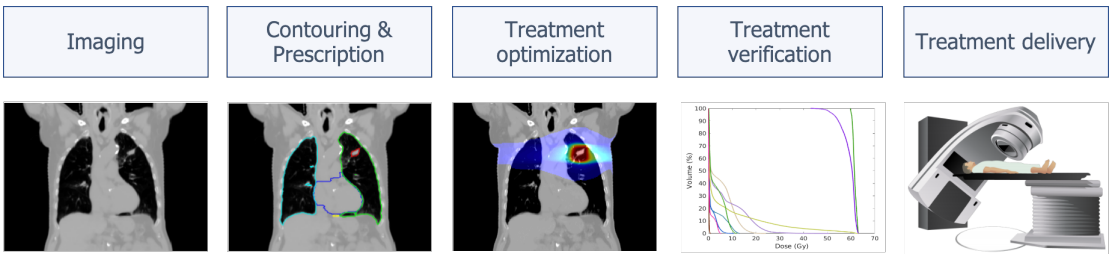

Figure 2.2: Clinical workflow of radiotherapy, adapted from [7].

2.2.1 Imaging

The first step in the clinical workflow is called the imaging step. This step consists of acquiring images of two-dimensional sections of the patient with a CT scan. Once all the images are acquired, then it is possible to reconstruct a three-dimensional volume of the scanned region of the patient [7].

2.2.2 Contouring and prescription

The second step in the clinical workflow can be divided in two phases. In the contouring phase, the physicist delineates the tumor and the other organs shown in the images acquired in the previous step. Then begins the prescription phase. In this phase, the physicist evaluates the dose ought to be prescribed depending on the tumor and surrounding organs. Depending on the organs, there are different constraints to fulfill. Generally, the constraints on the tumor are that the mean value should be equal to a given constant and that the minimum delivered dose should be greater than another constant. On the contrary, constraints for surrounding organs and tissue are typically that the maximum value should be less than a dose constraint while minimizing its mean dose. Other criteria on the treatment time or on conformity should also be considered [16]. The number of fractions is also evaluated in this step.

2.2.3 Treatment optimization

The treatment optimization step, as the name suggests, is the optimization of the treatment plan to ensure an optimal dose distribution, conform to the prescriptions given in the previous step. The treatment optimization in radiotherapy is a multi-criteria problem as it has to balance the dose between the tumor and the neighbouring organs with the aim to achieve the highest quality of life for patients. This problem requires an individualized solution for each patient as the anatomy of each patient is unique [16].

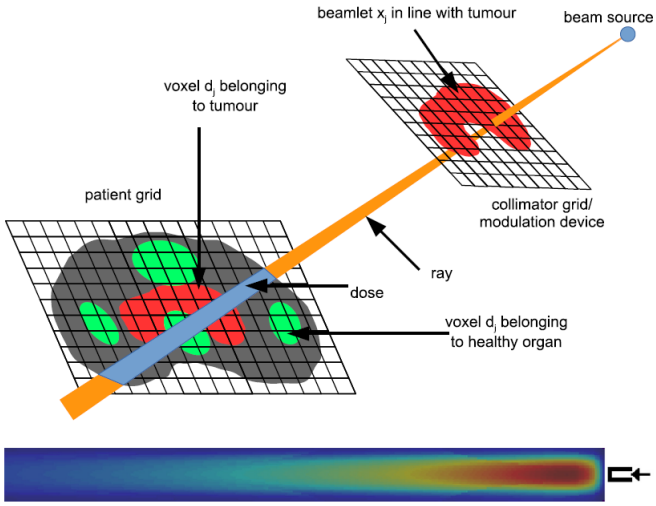

Figure 2.3: Representation of the radiotherapy problem decomposition. The beam arrives at the collimator grid where it is shaped and discretized into beamlets. The dose arrives in the organs in various quantities. The difference in dose intensity is the result of the different times of apertures of the collimator [16].

Fig.2.3 represents the numerical decomposition of the radiotherapy problem. In this figure, the beam reaches the multi-leaf collimator and is then discritized into beamlets. These beamlets are the decision-variables of the radiotherapy optimization problem. The numerical value of these variables is the intensity of the beam after passing through the grid. The intensity of the beam is then converted into dose when measuring a numerical value in the patient. The dose in the patient is related to the intensity of the beam by a a linear relation:

$$d = d(x) = Ax \tag{2.1}$$

In equation (2.1), d is the voxel dose, x is the intensity of the beamlet and A is called the dose-fluence matrix. This matrix can be computed by algorithms using the images obtained with the CT and the beam position.

Instead of optimizing the dose over the entire scanned volume of the patient, the dose is divided into volumes of interest and the dose of each volume is optimized separately. Therefore, the optimization problem can be written as follows as proposed by Breedveld et al. in[16]:

$$
\begin{aligned}
\text{minimize}_x \quad & f(d_1) \\
\text{subject to} \quad & g_1(d_2) \leq b_1 \\
& g_2(d_2) \geq b_2 \\
& g_3(d_3) \leq b_3 \\
& g_4(x) \leq b_4 \\
& x \geq 0 \\
\text{where} \quad & d_1 = A_1 x \\
& d_2 = A_2 x \\
& d_3 = A_3 x
\end{aligned} \tag{2.2}
$$

In equations (2.2), d_1, d_2 and d_3 are the doses in three different organs while $f()$ and $g()$ are the cost-functions. This problem consists of minimizing the dose delivered in the organ 1 according to a function $f()$. This minimization must consider that the dose in organ 2, probably the tumor, must have a dose between two constraints. A third structure is taken into account in this problem formulation. Finally, the constraint $x \geq 0$ ensures that the intensity of the beam stays positive [16].

Once this problem is solved, the physicist obtains a so-called treatment plan containing machine parameters settings needed to realize the desired dose distribution. It is then important to be able to compare different treatment plans. One technique able to quickly assess whether a treatment plan is of high quality is Dose-Volume Histogram (DVH). In DVH, each curve stands for a particular organ and reflects the proportion of the organ volume that receives that amount of dose. As observed on Fig.2.4, for organs at risk, the curves should remain as close to the left as possible, with a maximum of the volume receiving a zero dose. On the contrary, for the target volume, the curve should be on the right with a steep slope downward at the level of the prescribed dose.

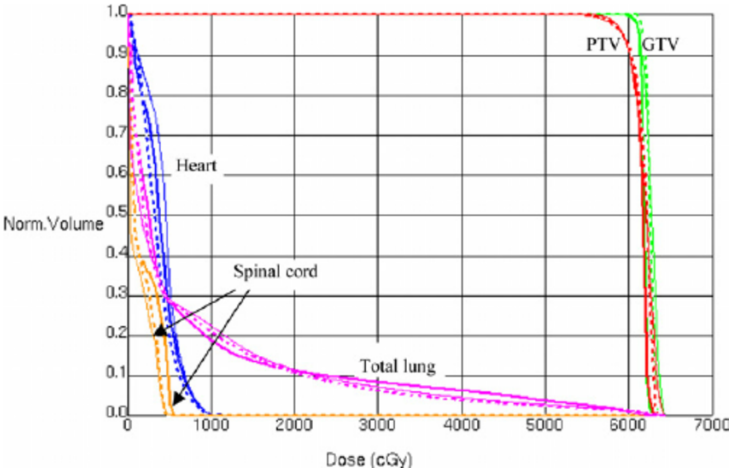

Figure 2.4: Dose-Volume Histogram for a lung cancer case. The dose delivered at the target (red and green curves) is on the right with a steep slope downward showing that a maximum dose is imposed. For organs at risk and surrounding tissue, the dose remains as left as possible [17].

2.2.4 Treatment verification

This is the final step before the treatment delivery. This is the step in which the oncologist checks that the treatment plan meets all the necessary requirements before validating it [7].

2.2.5 Treatment delivery

Finally, when the treatment plan is validated by the oncologist, it can be administered to the patient in several fractions. The number of fractions depends on each person, but generally, the patient will have more or less 5 sessions per week during 5 to 8 weeks [18]. Unfortunately, the delivery of radiotherapy is affected by numerous factors. It is possible for the patient to not be perfectly positioned. To avoid this as much as possible, visual tools are installed in the treatment rooms to position the patient the way he was during the imaging step. Moreover, it is possible that the patient anatomy changes in case of weight loss, tumor shrinkage or if the patient breathes. The dose delivery can also be affected by an imperfect conversion of imaging data into quantities needed to compute the dose distribution [7].

2.3 Particularity of proton therapy

Now that radiotherapy is fully understood, let's take a look at proton therapy. Proton therapy is a particular case of radiotherapy and the one we use in our approach. In this specific case, the charged particles are protons whereas conventional radiotherapy uses X-ray photons to treat the patient. The clinical workflow described above also applies to proton therapy. Actually, proton therapy has few advantages over conventional techniques of radiotherapy. The main one is being able to deliver the dose at a specific range thanks to the particularity of the Bragg peak.

2.3.1 Bragg peak

The Bragg curve is typical for heavy charged particles. This curve describes the energy loss of ionizing radiation during travel through matter. The Bragg peak is the maximum of this curve. You can observe the Bragg curve of X-rays, protons and carbon ions on Fig.2.5.

As shown in Fig.2.5, the X-rays, used in conventional radiotherapy, lose their energy very rapidly when they travel through tissue. The X-ray photons lose energy and deliver some dose all along their path. And, as set out by Fig.2.5, the dose delivered in the tissue located in front of the tumor is bigger than the dose delivered in the tumor. Behind the tumor, the dose delivered is smaller but still greater than null.

On the contrary, when protons enter the human body, the delivered dose is low. It then increases slightly with depth into the tissue. A significant increase occurs and forms a peak, the Bragg peak. At this peak, the delivered dose is very high and becomes zero after the peak. The particularity of the Bragg peak is the concept upon which proton therapy is based. Indeed, the purpose of proton therapy is to align the Bragg peak with the tumor to deliver a maximal dose in it while delivering a dose nearly null in the healthy surrounding tissue. As the range of this peak is very narrow, it is necessary to use proton

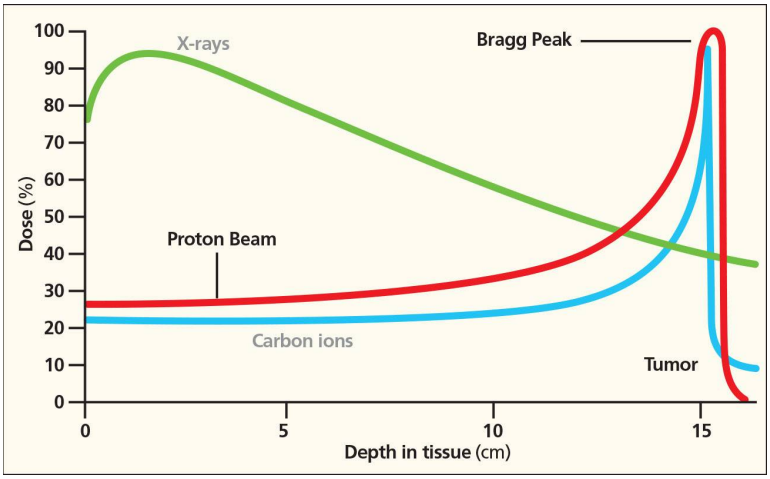

Figure 2.5: Comparison between dose distributions of X-rays (green), protons (red) and carbon ions (blue) [19].

beams with different energies in order to cover the whole volume of the tumor.

Thanks to the particularity of the Bragg peak, there are actually two main reasons for choosing proton therapy rather than conventional radiotherapy: higher dose to the tumor and fewer side effects. Proton therapy is suitable for tumors that need higher radiation dose. As the dose is mainly delivered within the tumor, there are less risks of toxicity of the healthy surrounding tissue. This is the reason why proton therapy is favored for treating childhood cancers. As it can target the tumor without damaging surrounding tissue, it reduces the risk of treatment induced disorders [20]. Nevertheless, proton therapy is not always prescribed as a treatment because it is much more expensive than any other kinds of treatment. This is because only few sites are equipped with proton therapy systems as these facilities are very expensive [21].

2.3.2 Different methods of proton therapy

Passive scattering

Passive scattering is the oldest method used in proton therapy and its system is represented on Fig.2.6. The first component is a range-modulator wheel. It allows to have protons of many different energies in the beam so that protons do not stop at the same depth but cover the whole depth of the target. The following two components of this device, both scatterers, are needed to focus the beam on the right direction and then to scatter it in the right way. The main component of this technique is the fourth one, containing a collimator and a compensator. This solid brass disk is placed near the patient and has an aperture matching the shape of the patient tumor. This aperture enables the protons to find the target as the protons are directed towards the tumor. This technique has some advantages, be very simple to use and being able to treat tumors on moving organs. However, this technique can not be used on a large scale as it requires patient-specific collimators and compensators. Moreover, some dose is delivered in the surrounding healthy tissue and also, the patient may absorb a significant quantity of neutrons that comes from the collision between protons and the brass [7].

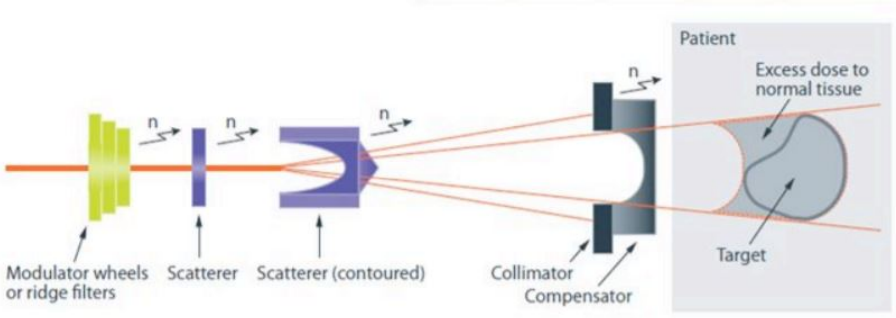

Figure 2.6: Scheme of the passive scattering system [7].

Pencil Beam Scanning

The Pencil Beam Scanning (PBS) method is a more advanced technology and consists of using a narrow pencil beam of radiation and steering it in accordance with the tumor shape [18]. This technique was developed so as not to need patient-specific collimators and compensators. Fig.2.7 shows a scheme with the essential components of the biomedical proton beam delivery system. In order to guide the proton beam, different kinds of magnets are used. First, a kicker magnet is used to switch the beam on and off by steering it into a narrow aperture or a beamstop. Then, the beam travels through focusing quadripoles to focus the beam in one direction. The beam is steered in the X-direction using a sweeper magnet, which is, actually, a dipole. After that, the beam travels along the beam pipe in which are four ionization chambers that monitor the total dose and the position. Once this is done, the beam arrives at a range shifter able to move the Bragg peak of the beam [18].

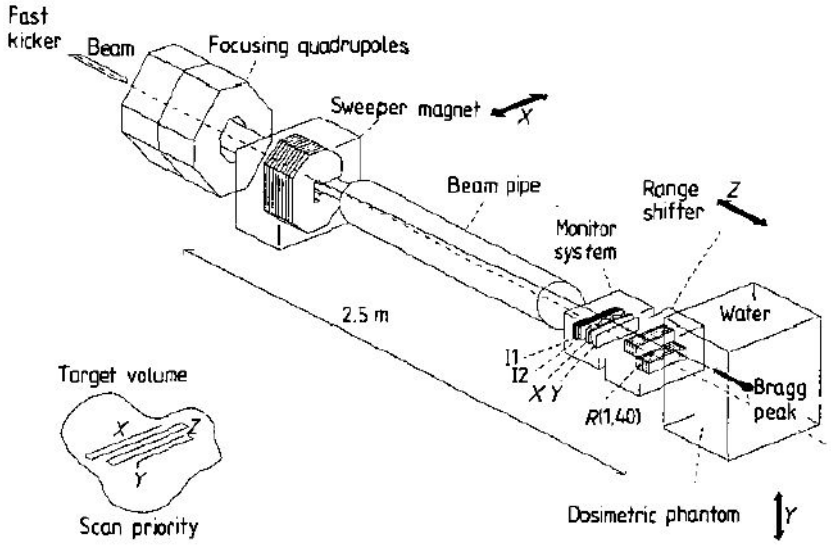

Figure 2.7: Scheme of the biomedical proton beam delivery system [18].

This beam delivery system operates as described above and scans the patient in discrete spots. Steering magnets are then used in order to bend the beam and adjust the beam trajectory along horizontal and vertical directions. To scan the whole target volume with this technique, it is essential to first scan a plane. This is then done using steering magnet. Once the plane is scanned, the Bragg peak is shifted by the range shifter so that the dose is delivered in another plane of the tumor. Typically, the first plane scanned will be the further one since some dose is delivered in the first layers of the tumor. Therefore, the energy of the first beam is the highest. The discrete spots delivery system is represented on Fig.2.8.

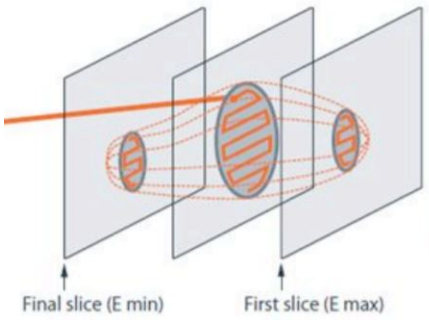

Figure 2.8: Discrete spots delivery system, adapted from [7].

When using PBS, different kinds of scanning techniques are available. These techniques vary in the way they deliver the dose to the tumor.

1. **Uniform scanning**: in this technique, each slice of iso-energy is scanned uniformly. This induces a flat dose in a homogeneous medium. But, it is necessary to use a range compensator when using this technique with a heterogeneous medium.

2. **Intensity-modulated proton therapy**: the principle of this technique is the same as intensity modulation explained for radiotherapy. The difference between both techniques is that, in proton therapy, it is important to consider the Bragg peak. Since the delivered dose in front of or behind this peak is nearly equal to zero, it is important that this peak happens in the volume of the tumor.

The discrete spots delivery system of the PBS gives this method a huge advantage in regards to passive scattering as it does not require patient-specific collimators and compensators. But, unfortunately, PBS is not robust when used with target on a moving organ as it does not treat the entire volume of the target simultaneously. This phenomenon is the principal disadvantage of this technique. It is defined as the **interplay** and will be detailed in the next chapter.

2.3.3 Benefits of proton therapy for lung cancer

As seen before, proton therapy has few advantages compared to conventional radiotherapy. This advantages are also present for lung cancer. First of all, as proton therapy reduces the dose delivered to normal tissue, the treatment toxicity is lower. Moreover, this treatment enables a higher chance of cure which is not attainable with photon treatment or chemotherapy alone. This highest chance of recovery results from a safer delivery high-dose radiation to the tumor, but not to the surrounding tissue. As far as lung cancers are concerned, it is particularly important to take care of these surrounding tissue as they are the heart or the spinal cord. Finally, it has been demonstrated that proton therapy combines better with other treatments like chemotherapy and surgery [22].

Chapter 3

Interplay

3.1 Definition

As described previously, lung cancer is a specific type of cancer. The tumor has the particularity to be on a moving organ which leads to a motion of the tumor. And, it has been proven that, for targets that move during the treatment (using radiation therapy), there is an interference between dynamic pencil beam delivery and target motion. This phenomenon is called the **interplay**. The interplay leads to a non-uniform delivered dose in the tumor, usually manifested in local under-dosage and over-dosage regions [23]. As a result, the interplay effect has a negative impact on the cancer treatment with radiotherapy. Indeed, in order to treat the tumor in the right way, it must receive an uniform dose in the prescribed amount on its whole volume.

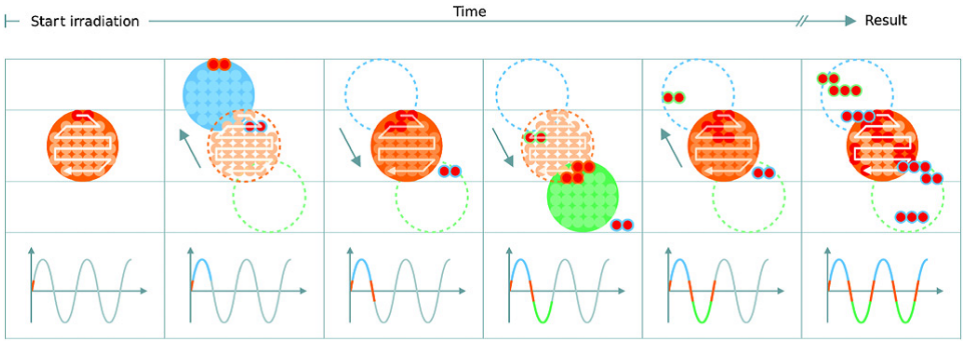

Figure 3.1: When the tumor moves, it results in local zones of under-dosage and over-dosage in the tumor [23].

Fig.3.1 displays the effect of the interplay on a moving target. As shown in white, the beam is scanning a volume spot by spot with a serpentine movement. At the beginning of the irradiation, the beam and the tumor are synchronized, the beam reaches the tumor and delivers a dose within the tumor volume, the two red points. But, when the patient breathes, the tumor moves and reaches a particular location shown in blue in the second sub-figure. At this particular anatomy, the beam does not reach the tumor and the dose is delivered outside the tumor volume, hitting some surrounding healthy tissue. This is represented by the two blue encircled red points. As the patient continues to breath, the tumor comes back to its initial position where it is in phase with the beam and, the beam reaches the tumor volume again. This phenomenon is repeated throughout the treatment, resulting in under-dosage and over-dosage of certain tumor areas and irradiation of surrounding healthy tissue.

3.1.1 Factors influencing the effect of the interplay

Bert et al. have demonstrated in [23] that the effect of the interplay is impacted by few factors. They are the same for every patients but the effect is unique to each.

- **Target motion characteristics**: these characteristics depend on each patient as they are the motion's amplitude, period and its initial phase.
- **Motion direction**: when considering the usual line-by-line scanning motion of the beam, the target motion can be horizontal or vertical. So, the target motion can be parallel or perpendicular to the motion beam scanning.
- **Scan speed**: this speed influences the number of spots scanned by time units.

Target motion characteristics

Fig.3.2 displays the interplay effect for different target motion characteristics. As shown in Fig.3.2a, in the case of a stationary target, the dose delivered in the Region Of Interest (ROI) is uniform. Unfortunately, the conclusion is far from being the same for a mobile tumor. In the 15 other cases, target motion characteristics vary while the motion direction of the target is always parallel to the fastest motion of the beam and the scan speed is also always the same.

In the 15 non-stationary cases, under-dosage and over-dosage zones in the ROI are represented by, respectively, a darker and a lighter grey than in the stationary case, as displayed in Fig.3.2b. Moreover, when the target is moving, it results in bands that extend beyond the ROI. Fig.3.2 demonstrates that the target motion characteristics influencing the dose uniformity the most is the motion amplitude. The higher the motion amplitude of the target is, the larger the extensions over the ROI become and the more present local zones of under-dosage and over-dosage in the ROI are. This is represented in Fig.3.2c.

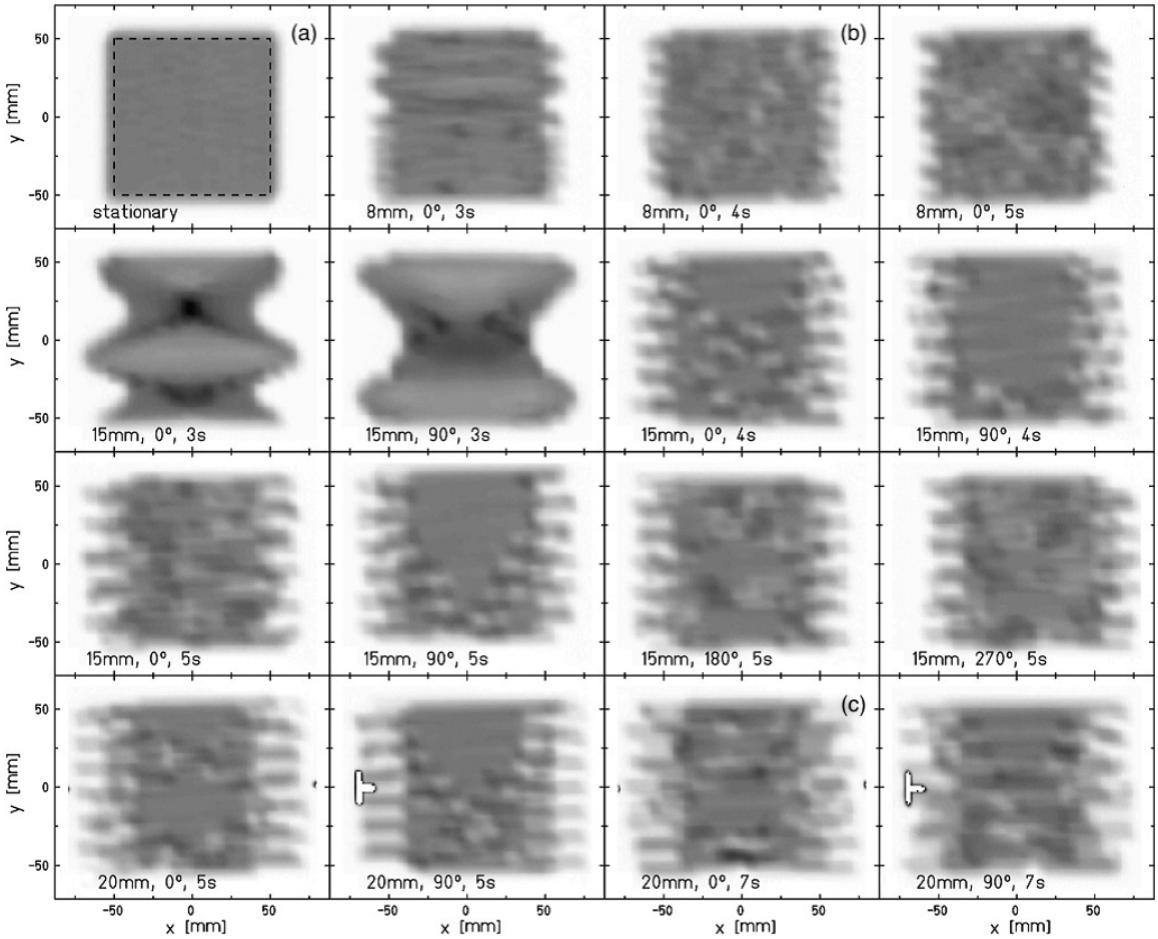

Figure 3.2: Influence of the target motion characteristics on the effect of the interplay. The amplitude varies between 8 and 20 mm, the period between 3 to 7 s and the initial phase between 0° and 270° [23].

Motion direction

Fig.3.3 illustrates the effect of a change in direction of the target motion. As displayed on Fig.3.3b, when the motion of the target is perpendicular to the fastest motion of the beam, the interplay effect results in diagonal tapes. The slope of those diagonals is determined by the ratio between the velocities of scanning and target motion. Moreover, it can be noted that, despite the non-uniform dose, it is mainly delivered in the ROI. On the contrary, as set out previously, when the target motion is parallel to the fastest motion of the beam, as on Fig.3.3c, it results in horizontal stripes of under-dosage and over-dosage. And those horizontal stripes extend beyond the ROI [23].

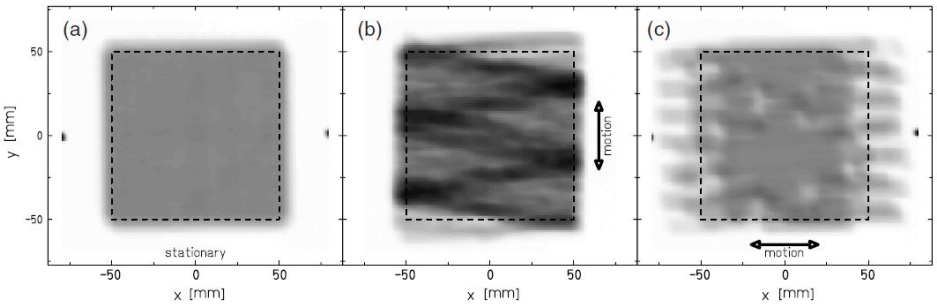

Figure 3.3: Effect on the interplay pattern caused by the motion direction, (b) perpendicular versus (c) parallel to the direction of motion beam scanning [23].

Scan speed

Fig.3.4 displays the effect of various beam-scanning speeds on the interplay pattern. In those three experiments, the motion of the target was orthogonal to the motion of the fastest motion of the beam. For those three cases, it is easy to see the typical interplay pattern with the diagonal stripes presented above. Moreover, it is important to observe that this pattern remains quite the same for the different motion beam-scanning velocities. Besides, the pattern becomes like a grid when the scanning speed increases.

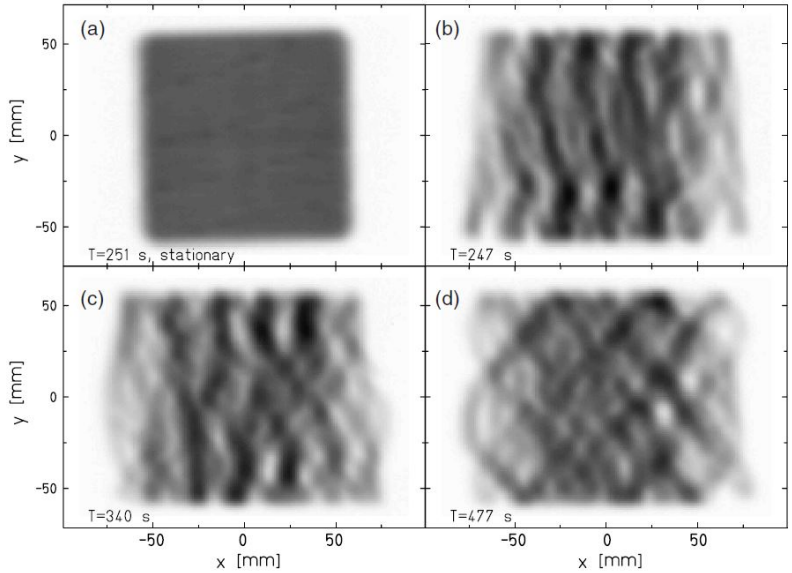

Figure 3.4: Impact of the scan speed on the delivered dose in the region of interest when the target motion and beam motion are perpendicular [23].

3.2 State of the art

Now that the concept of interplay is understood, it is time to explain how to minimize this negative effect. Nowadays, many different methods have been studied in order to mitigate the effect of the interplay. Some of those techniques are clinically available, but some of them are still in a research phase. In this section, we will introduce the most common ones.

3.2.1 Respiratory gating

Respiratory gating is probably the oldest and most extensively studied technique. The principle of respiratory gating is extremely straightforward but quite complicated to implement. It consists of switching the beam on and off at particular points during the respiratory cycle. This can be done with the help of an external surrogate. The external marker continuously monitors the patient's respiratory cycle, giving a trace of the respiratory cycle. As a result, selecting the respiratory phase for the treatment delivery is possible. The beam will then only be switched on during this respiratory phase.
Unfortunately, this technique has some major flaws [24]:

- **Geometric uncertainty**: even though it has been proven that the abdominal surface motion is well correlated with the motion of internal anatomical structures, it can arrive that the predicted tumor position is not the real one because of non-breathing related changes between the planning image and the treatment day. In such case, the treatment planning is based on a wrong tumor position, therefore the dose is delivered in the wrong place.

- **Long time delivery**: as the beam is only switched on during the selected respiratory phase, the beam is switched off during around 80% of the respiratory phase, inducing a longer treatment. However, the longer the treatment is, the higher the risks of movement from the patient are. Consequently, the higher the risks of dose delivery errors are. Longer treatment also leads to a loss of profit.

- **Selected respiratory phase**: there are two schools of thought on the phase in which the dose ought to be delivered: selecting end-inspiration and selecting end-expiration. According to the end-inspiration advocates, the main pro is that the lung is at maximum expansion, avoiding delivering dose in healthy tissue. However, the tumor remains at this phase during a very short period which leads to a small treatment window. On the contrary, according to end-expiration advocates, the main advantage is that the treatment window is longer as the tumor remains a long time in this configuration. However, the main downside is that the lung is compressed.

3.2.2 Fractionation

The principle of fractionation is very simple. It consists of giving the whole dose in a certain number of treatment sessions instead of giving all the dose at once. Fractionation is based on the principle that healthy tissue recovers faster from radiation than cancerous cells [16]. This technique has many benefits [25]:

- **Repair of sublethal damage**: sublethal damage[1] becomes lethal if accumulated. This reparation is more important for healthy cells than for cancerous ones.
- **Reassortment of cells within the cell cycle**: because of the high radiosensitivity of the G2 phase[2] of the cell cycle, cells are blocked in this phase when they are irradiated.
- **Repopulation**: this is the cell proliferation between two sessions. This proliferation is profitable for healthy cells as it limits the toxic effects of the radiation on the healthy surrounding tissue. But, this repopulation is detrimental for cancerous cells.
- **Reoxygenation**: well-oxygenated cells are radiosensitive and are eliminated when they are irradiated. Thanks to fractionation, hypoxic cells will become well-oxygenated and will become radiosensitive.

Phillips et al. in [18] study the effect of fractionation on dose uniformity with respiratory motion. As set out by Fig.3.5, the percentage standard deviation of the dose decreases when the number of fractions increases. This effect is demonstrated for three different respiration amplitudes. This shows that a higher number of fractions leads to a more uniform dose.

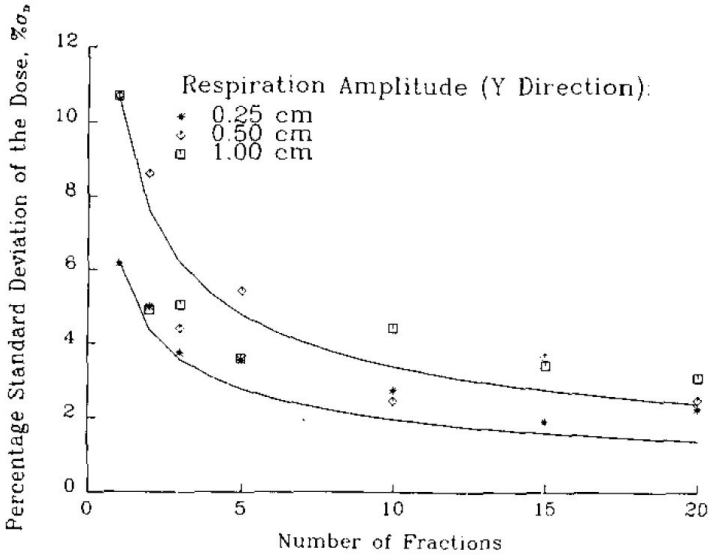

Figure 3.5: Percentage standard deviation of the dose as a function of the number of fractions. This percentage standard deviation decreases like the square root of the number of fractions, as represented by the two solid lines [18].

[1] A sublethal damage is produced in an irradiated cell. This lesion does not induce cellular death on its own, but can induce it as they accumulate [26]

[2] Phase of the cell cycle in which the cell uses the transcribed DNA in order to make all the proteins in greater quantity so that at the time of division, everything is available for the two new cells [26]

3.2.3 Repainting

The repainting technique has been widely studied and is probably the easiest to apply clinically. The technique of repainting, also called re-scanning, can be split in two sub-techniques [27]:

- **Volumetric re-scanning** consists of irradiating the complete volume once before the beginning of the next scan.
- **Non-volumetric re-scanning**, also called layered re-scanning, consists of scanning multiple times the same iso-energy layer before changing the energy to scan another slice [28]. There are two approaches used to deliver the dose in each scan. In the first one, called scaled re-scanning, the delivered dose to a spot in one scan is equal to the total dose divided by the number of re-scans. In the second technique, iso-layered re-scanning, the duration of irradiation is limited by a maximum value.

The choice between both different re-scanning techniques relies on the treatment machine as well as on the dynamics of the motion of the target to be treated [29]. Repainting achieved good results. Unfortunately, the number of re-scans needed to obtain an acceptable dose homogeneity is unknown and depends on the patient's anatomy. It has two main disadvantages: it can not be automated and can lead to long delivery times [27].

3.2.4 Security Margin

This method is very common and is used to take into account geometrical uncertainties. In order to ensure an uniform delivered dose within the target, security margins consist of enlarging margins around the tumor. However, this technique has one main flaw: a larger target volume means that the healthy surrounding tissue is reached, and the dose accumulates into it [30].

Here are two ways to compute these margins [31]:

- **Population-based margins**: computation of the margins around the clinical target volume so that 95% of the target dose is delivered to at least 90% of the patients.
- **Individualised margins**: computation of the margins taking into account the time-average position of the tumor and the standard deviation of the motion amplitude for the patient.

3.2.5 Real-time tumor tracking

Real-time target tracking is the most studied technique used to mitigate the interplay effect. Many studies have been carried out to manage the tumor tracking, but currently, it is not yet clinically available in particle therapy [27]. The real-time tumor tracking problem can be divided in two sub-problems: the target localisation and the dynamic adjustment of the beam.

Target localisation, as the name suggests, consists of tracking the position of the tumor throughout its entire motion in real-time. Many approaches are used to have real-time information about the target localisation:

- **Marker-based imaging**: in this case, markers are implanted inside or close to the tumor and they can be easily visualised with an imaging method. Results have demonstrated that the use of markers decreases the dose deviation of up to 82%. Unfortunately, the number of remaining errors is still too high when using an active dose delivery system [30].
- **Markerless imaging**: in this case, there is no implanted marker to have information about the target localisation. Instead, this kind of methods consists of using fluoroscopic imaging [30], and more recently MRI images with the development of MR-Linac hybrid machines [32], to continuously locate the target.
- **External markers**: for this technique, external markers are used to provide information about the target localisation. It has been demonstrated that the abdominal surface motion is well correlated with the motion of internal anatomical structures induced by breathing.

In order to achieve the real-time tumor tracking, it is important to be able to adjust the direction of the beam according to the new position of the target.

3.2.6 Spot sizes

Another kind of studies carried out to mitigate the interplay effect concerns the size of the spot delivered by the beam. Grassberger et al. in [33] characterized the dosage on the tumor volume depending on the size of the spot. For that purpose, they used two types of spots: a small one and a big one. The width of the small spot is 3 mm while the big one's is 13 mm.

The results of this study are displayed on Fig.3.6. Fig.3.6(left) and Fig.3.6(right) represent the absorbed dose and the percentage of the prescribed dose it is, as a function of the target motion amplitude for respectively big and small spots. When considering only one fraction, Fig.3.6 shows that big spots provide better result when the target motion is large. In such configuration, the minimum delivered dose corresponds to 78% of the prescribed dose while it is equal to 48% for the small-sized spots. But, the result is not the same at the end of the multi-fractions treatment. As shown with the closed symbols, the results for small-sized spots are better: for every motion amplitude, the percentage of the average dose delivered in the target is nearly equal to 100%. The standard deviation of the dose delivered is lower with small spots, leading to a more uniform dose [33].

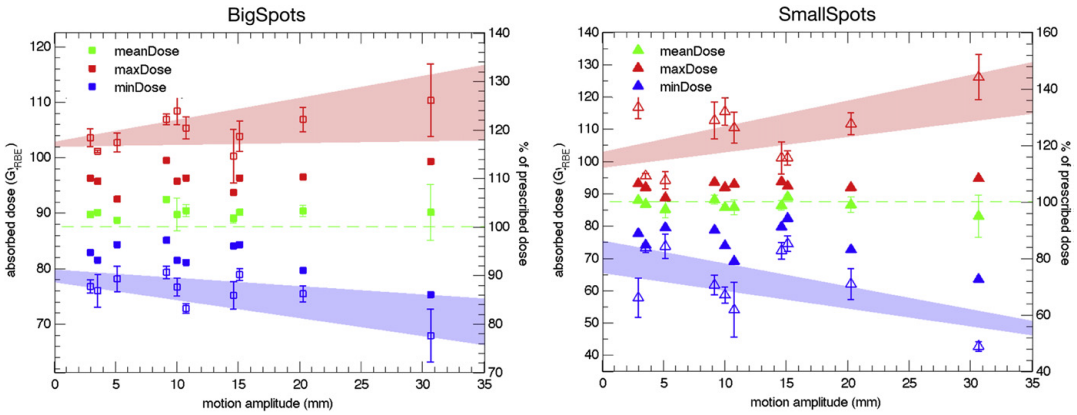

Figure 3.6: Influence of the spot size on the dose delivered in the target volume [33]. The closed symbols stand for the n-fractions experiment while the open ones are the 1-fraction results.

3.2.7 Offline correction of the beam delivery

Although this technique is rather recent, it has already been applied in clinic. In contrast to respiratory gating, this method irradiates the target volume during the whole respiratory period. The aim of this method is to obtain an uniform dose distribution thanks to an uniform irradiation. To achieve this uniform irradiation, an algorithm computes the relative beam weight delivered in each respiratory phase and determines which phases receive the largest amount of dose during the fraction. Then, for the next fraction, those phases are skipped and the dose will only be delivered in smaller weight-phases. After this second fraction, the algorithm recalculates the new beam weights and other phases will be skipped at the next treatment session [34].

The results of this method are displayed on Fig.3.7. On Fig.3.7b, it can be noted that with offline correction, 99% of the target volume receives 100% of the prescribed dose, whatever the value of this dose. On the contrary, in case of a lack of adaptation, the percentage of dose received by 99% of the target volume is lower and it decreases with a larger prescribed dose [34].

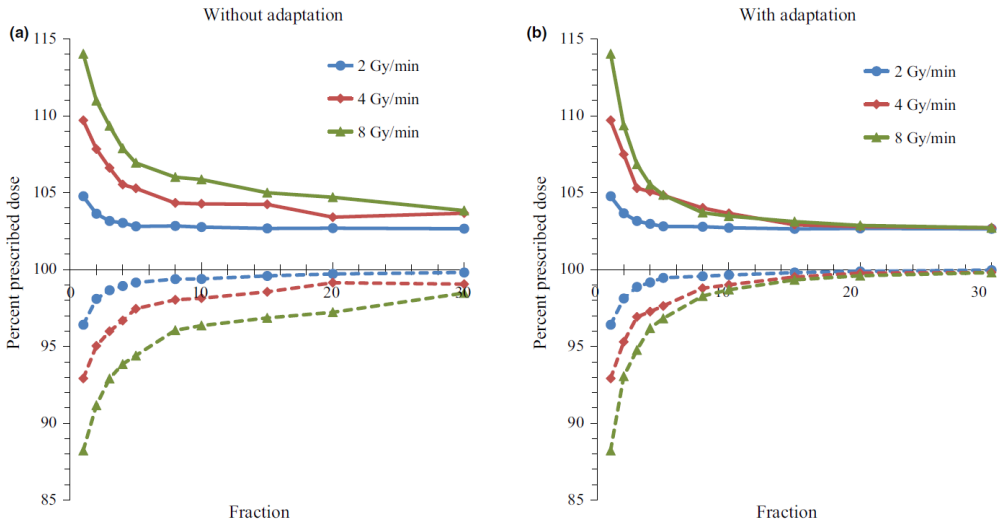

Figure 3.7: Comparison of the dose delivered in the target volume (a) without adaptation versus (b) with adaptation. Solid lines = $D_{1\%}$ (Dose delivered to 1% of the target volume), dash lines = $D_{99\%}$ (Dose delivered to 99% of the target volume) [34].

3.2.8 Optimizing the spot delivery sequence

A study was done to optimize the sequence of the beam. Actually, the optimization consists of maximizing the area covered by the proton beam in any respiratory period. This method is represented on Fig.3.8. Fig.3.8a shows the classical scanning movement, Fig.3.8b and Fig.3.8c represent the regular delivery scanning sequence. In those cases, the interval between two consecutive spots is not optimized. As a result, as displayed on both Fig.3.8b and Fig.3.8c, the dose is delivered outside of the target when the motion of the beam is not synchronized with its motion [27]. On the contrary, Fig.3.8d and Fig.3.8e represent the optimized beam sequence. In those cases, the interval between two consecutive spots is optimized. As a result, the target is reached for both respiratory phases. For both cases, the number of spots delivered during a particular anatomy is constant.

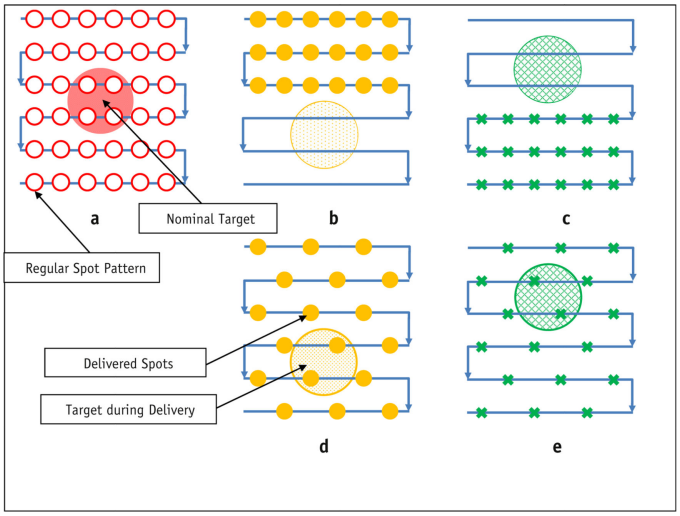

Figure 3.8: Optimization of the dose delivery process. (a) is the nominal plan; b) and c) show the regular delivery sequence; d) and e) display the optimized delivery sequence [27].

The results of this technique are represented on Fig.3.9. This figure shows the percentage of the dose delivered in the tumor volume. As shown in green, the dose delivered with the Optimized Sequence (OS) is more homogeneous as a larger distance has received a 100% relative dose. With the other two techniques, Worst Sequence (WS) and Regular Scanning (RS), the relative dose deposited in the tumor is more heterogeneous. There are local over-dosage and under-dosage zones.

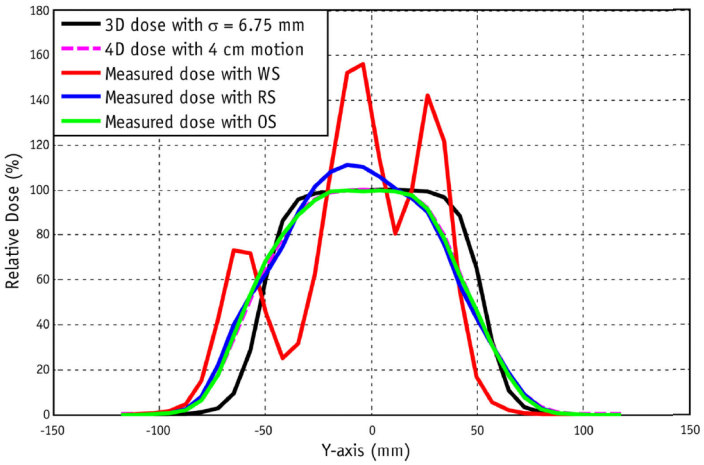

Figure 3.9: The black solid line represents the three-dimensional dose distribution for the optimized sequence. The dotted line is the four-dimensional dose distribution with a motion amplitude of 4 cm and a period of 10 s. Colour solid lines display the measured single-fraction delivered dose using Worst Sequence (red), Regular Scanning (blue) and Optimized Sequence (green) [27].

The results of this study demonstrated that the optimized delivery sequence reduces the heterogeneity of the dose delivered in the target, and this no matter the respiratory motion amplitude. The con of this method is that it requires a postprocessing of treatment plans.

3.3 Summary

In this chapter, we have defined the interplay phenomenon caused by the use of the PBS dose delivery method with a target localized on a moving organ. Moreover, we have seen the different methods used to mitigate the effect of this phenomenon. Table 3.1 summarizes the pros and cons of each method described above.

Table 3.1: Pros and cons of the different methods already studied to mitigate the interplay phenomenon.

	Pros	Cons
Respiratory gating	- Switches the beam on and off - Follows the respiratory cycle	- Difficult to implement - Geometric uncertainties - Long delivery times
Fractionation	- Sacrifices fewer healthy cells - More uniform dose with a higher number of fractions	- Dose is delivered during many sessions
Repainting	- Easy-to-implement	- Required an unknown number of rescans
Security margins	- Target is completely reached	- Healthy surrounding tissue is also reached
Tumor tracking	- Dynamic adjustment of the beam - Knowledge of the target's position	- Many mistakes - Not yet clinically available
Spot sizes	- Adapts to different tumor sizes	- Results depend on the number of fractions
Offline correction	- Considers the previous fractions	- Requires recalculation between each fraction
Optimizing spot delivery	- Hits the tumor at each phase of the respiratory cycle	- Reaches healthy surrounding tissue

Chapter 4

Real-time decision making

All the already experimented methods show the difficulty to deliver the right dose, at the right time and in the right place. This is mainly due to the fact that computations are not performed in real-time. In these different methods, the dose is delivered according to the treatment plans determined by the physicists during the treatment planning phase and they often do not consider the patient's anatomy at the time of dose delivery. This work includes a maximum of advantages of techniques known to reduce the effect of interplay. We consider it important to draw inspiration from methods with promising results rather than to start from scratch. Table 4.1 highlights, on the left, the pros of the various methods developed in the previous chapter and on the right, how they were exploited.

Table 4.1: Pros of already studied methods used to mitigate the effect of interplay and how those features were implemented in this work.

	Pros	Implemented features
Respiratory gating	- Switches the beam on and off - Follows the respiratory cycle	- The beam can be switched on and off according to constraints
Fractionation	- Sacrifices fewer healthy cells - More uniform dose with a higher number of fractions	- The dose is delivered into 25 fractions
Repainting	- Easy-to-implement	- The target can be rescanned
Security margins	- Target is completely reached	- Small security margin around the target
Tumor tracking	- Dynamic adjustment of the beam - Knowledge of the target's position	- Target's position is known in real-time - The beam can be dynamically adjusted
Spot sizes	- Adapts to different tumor sizes	- Spot size is optimized
Offline correction	- Considers the previous fractions	/
Optimizing spot delivery	- Hits the tumor at each phase of the respiratory cycle	- The dose's delivery process is optimized

The main specificity of this work is the real-time decision making. This aspect sets our method completely apart from previous ones. This means that the dose computation and the place to deliver it will be continuously reassessed to take into account the mobility of the lung, of the tumor and of the surrounding organs at risk. The dose accumulated during the previous steps will also be considered. The choice of the way the dose is delivered inside the tumor will therefore be made in real-time, as the patient is on the table.

The other particularity of this work is the numerical simulation. By definition, a numerical simulation involves running a computer program in order to simulate a real and complex physical phenomenon. It is used to study the functioning and properties of the system under analysis and to predict its evolution [35]. In this work, we had to create a whole environment to best represent a lung tumor with surrounding organs that are moving due to respiratory motion. Based on this system and its evolution, the dose delivery will be evaluated in order to obtain a dose as homogeneous as possible within the tumor.

To carry out this work, the design of a complex computer program was necessary. Fig.4.1 shows the global architecture of the simulation. The computer program can be divided in two main parts, called materials and methods.

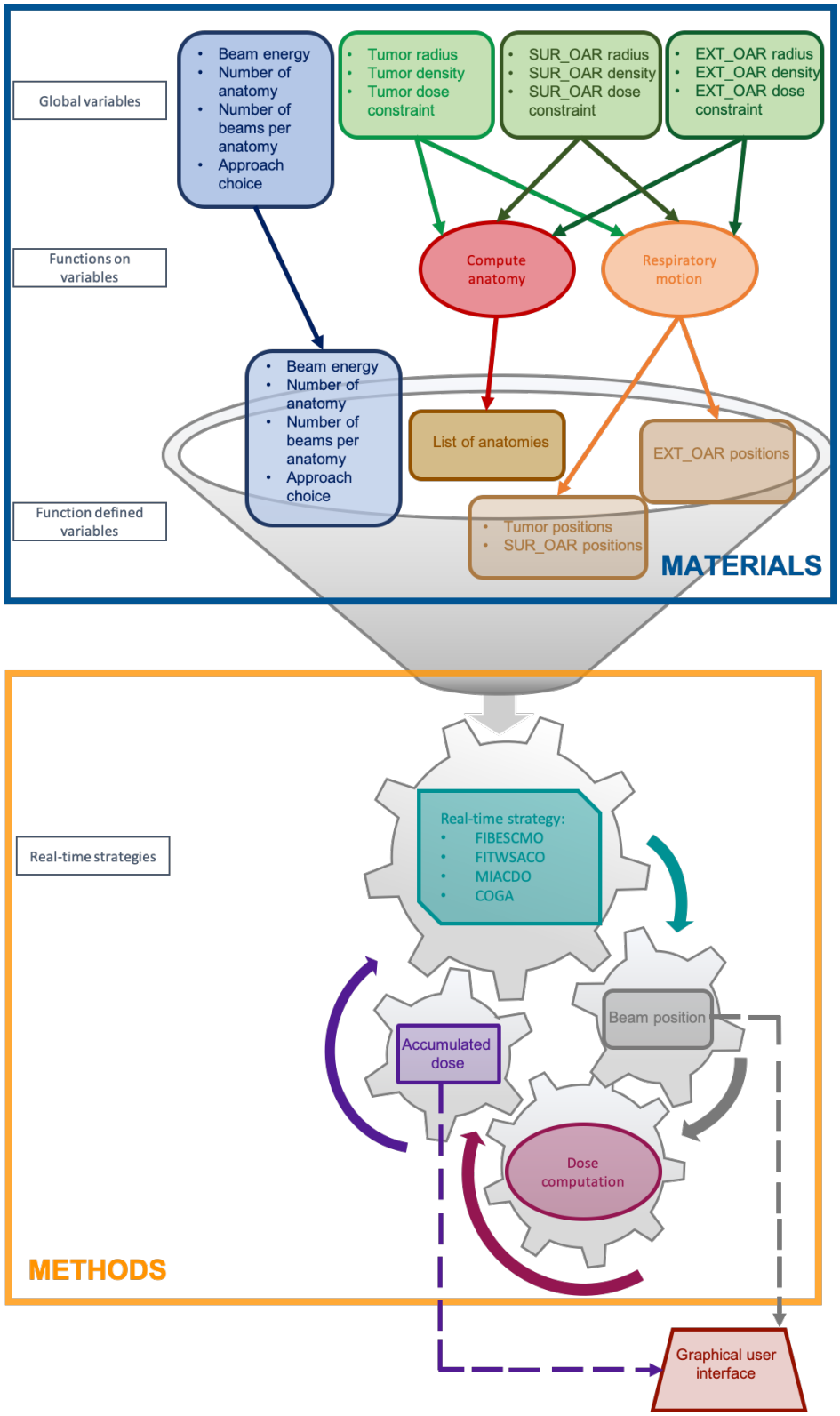

Figure 4.1: Overview of the different components of the simulation.

4.1 Materials

To carry out this simulation, we had to create all the different structures in order to simulate as well as possible the environment we wanted to reproduce, the dose delivery in a tumor located on a lung that is moving. In addition, a graphical user interface was created to observe the simulation process.

4.1.1 Anatomies

First of all, we had to simulate the different anatomies. In our case, we considered that the anatomies are composed of various spherical organs, representing a tumor and some organs at risk. Moreover, those structures move with the breathing. The respiratory motion will be described here under, in 4.1.1-Respiratory motion.

Tumor

The main item of our simulation was, obviously, the tumor. The tumor is described by a diameter, the position of its centre and also a density. Moreover, the tumor is characterized by a constraint on the dose delivered in its volume.

To determine the tumor's geometrical features, [36] and [37] were used. Both show that the size of the tumor depends on the stage of the cancer. The more advanced the disease is, the bigger is the tumor. In the first stage, the size of the tumor is smaller than 3 cm while in a more advanced stage, it is between 4 and 5 cm. In our simulation, the in-between size was used, this means a tumor of 35 mm.

For the constraint on the dose, we considered that the tumor must receive 50 Gy in 25 fractions, which means a dose of 2 Gy per fraction. Ideally, 95% of the tumor volume must receive this dose, but in our simulation we considered that the treatment fraction was complete when the mean dose in the tumor was equal to 2 Gy.

Table 4.2 shows the different values chosen for the tumor in order to have a realistic approximation.

Table 4.2: Tumor parameters used to have a realistic approximation.

	Density [g/cm^3]	Diameter [mm]	Dose constraint [Gy]
Tumor	0.7	35	$D_{mean} = 2$

Organ At Risk (OAR)

In order to have a simulation as real as possible, we had to consider organs at risk. In our simulation, we envisaged two kinds of organs at risk: surrounding and external structures. The particularity of those organs at risk is that we can decide, before running the program, whether to put them on or not. The surrounding OAR surrounds the volume of the tumor as it is the case for the lungs in real situation. On the contrary, the external OAR is totally independent from the tumor as, for example, the heart. Just like the tumor, they are characterized by a density, a size, a motion and a constraint on the dose. In addition, the external OAR is always positioned between the origin of the beam and the tumor.

In this work, the geometrical parameters of the organs at risk were not really based on the reality. In order to keep the size of the simulation grid small, we had to reduce the real dimensions of the organs. This is the reason why a surrounding OAR with a radius equal to twice the radius of the tumor and an external OAR of roughly the same size as the tumor were considered.

In contrast, it was important to put constraints as real as possible in order to simulate the dose situation as well as possible. As already said, we considered the surrounding OAR to be the lungs and the external one being the heart. In [38], Noël et al. consider the following constraints:

$$\begin{aligned} &\text{Lungs} && V_{20Gy} \leq 35 - 37\% \\ & && D_{mean} \leq 20Gy \\ &\text{Heart} && V_{30Gy} \leq 100\% \\ & && V_{45Gy} \leq 66\% \\ & && V_{60Gy} \leq 33\% \end{aligned}$$

Therefore, the constraints used in this work take into account these previous constraints but they were slightly adapted to include the simplifications in geometry. Moreover, we considered that the dose was delivered using 25 fractions.

All chosen parameters for both types of organs at risk can be visualized in Table 4.3.

Table 4.3: Features of the OARs used to have a realistic approximation.

	Density [g/cm^3]	Diameter [mm]	Dose constraints [Gy]
Surrounding OAR	0.5	65	$D_{mean} < 0.8$
External OAR	random(1,2)	25	$D_{mean} < 1.2$

Respiratory motion

As one of the main objective of this work is to control the interplay phenomenon, it was crucial to simulate the respiratory movement of the organs.

To represent this motion, we considered an elliptical movement with random noise. Depending on the number of anatomies studied over a respiratory period, we obtained various points belonging to an ellipse. The points of the ellipse were chosen to make sure that the whole volume of each organ remained in the grid. To introduce a timing parameter in this motion, a respiratory motion of 4 s was considered.

For the tumor and the surrounding OAR, the points were identical because we considered that they always have the same centre. On the other hand, the different positions of the external OAR were completely independent while also following an elliptical movement. Fig.4.2 displays the movement of the organs centres caused by breathing.

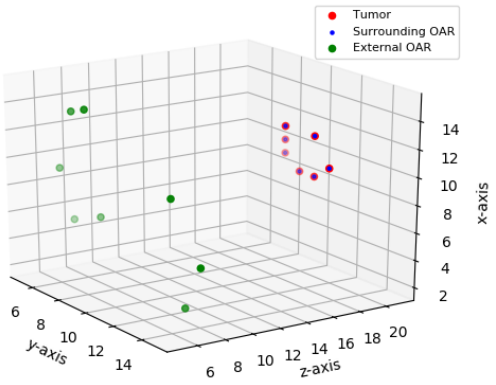

Figure 4.2: Representation of the respiratory motion. The positions of the surrounding OAR and the tumor are the same while the external OAR has a completely independent motion. This organ is always located between the origin of the beam and the tumor.

4.1.2 Proton beam

A proton beam is usually composed of many particles. This number must be high enough to deliver a smooth dose within the target. However, the computation with a high number of particles is time-consuming. This is why, in this work, the chosen number of particles is a compromise. It is limited to make sure that the computation is performed in real-time. Moreover, we considered a fixed monitor unit. The spot size used in this work is also a compromise. As shown in Appendix A.1, the dose delivery process largely depends on this size. In this work, the spot size is chosen in the middle of the two extremes in order to get the best results.

The initial mean energy of the beam is set at 200 MeV to approximate values used clinically. In fact, the beam energy is continuously reevaluated so as the majority of the Bragg peaks are located inside the tumor volume. This will be explained in more detail in 4.2.2-General Implementation. In this work, the direction of the beam is deemed to be constant and equal to (x,y,z) = (0,0,1).

Moreover, we consider that it takes 8 ms to deliver the dose in the desired spot and we estimate that a change of energy, when required, lasts about 1 s.

The different parameters of the beam are summarized in Table 4.4.

Table 4.4: Proton beam parameters used to have a realistic approximation

	Initial mean energy [MeV]	Number of particles	Monitor Unit	Beam direction	Spot size [mm]
Proton beam	200	50	10^9	(x,y,z) = (0,0,1)	$\sigma_x = 2$ $\sigma_y = 3$

4.1.3 Graphical User Interface (GUI)

The GUI lets us visualize how the simulation is running and how the algorithm chooses to deliver the dose. We have an idea of the system's evolution. As shown in Fig.4.3, it is divided into 5 sub-figures. Each sub-figure is important because it displays information essential for understanding the simulation.

The top three black and white figures are in the same group because they are used to represent the same type of information. Each of these figures is in a plane of space and is used to visualize the movement of the tumor and of the two organs at risk in that plane. The displacement in (x,y) is represented on Fig.4.3a, the one in (y,z) is on Fig.4.3b and the motion in (x,z) is on Fig.4.3c. In all three cases, the plane shown is the one passing through the centre of the tumor. It is important to know how the tumor acts because its movement is what makes the treatment difficult. Fig.4.3b and Fig.4.3c show whether the external OAR is in the field of view of the beam or not.

Furthermore, these three figures demonstrate how the strategy is carried out, i.e. which beam positions are selected and among these which are shot and which are not. For this purpose, those three figures have the same color code: a fired beam is shown in green whereas a not shot beam is shown in red. In Fig.4.3a, we can see which positions are selected and among them, which are fired. Fig.4.3b and Fig.4.3c show where the different beams stop. This is where the Bragg peak occurs. Based on this, the control of the beam energy can be done correctly.

The two bottom figures show how the dose accumulates in the different organs. This information is obviously crucial because it tells if the strategy delivers a homogeneous dose in the volume of the target. Fig.4.3d is divided in two. On the left, the accumulated dose in the central plane of the surrounding OAR and of the tumor; on the right, the accumulated dose in the external OAR. These figures show the accumulated dose in the reference anatomy, i.e. the first anatomy. The dose received by each of the organs during the current anatomy will first be translated into this reference anatomy before being accumulated to the dose delivered during the previous anatomies. Fig.4.3d is accompanied by a color bar linking each color to a specific dose value.

The last figure, Fig.4.3e, is equally important because it displays the Dose-Volume Histogram over time. This figure tells at any time how the dose is delivered in the different volumes. It helps to visualize the maximum dose or the dose received by a large portion of the target volume. In addition, this figure also displays the constraint on the dose in each organ. Therefore, we see when the constraint is no longer respected and how the algorithm adapts to respect it as well as possible.

In addition to these 5 figures, the GUI also displays additional information at the top of the screen. On the left, different times can be found. For example, the time spent changing energy, searching or shooting. In the middle, the information indicates the performed action. This can be "Searching for spots to shot", "Changing energy" or "Treatment Over". Finally, on the right are the number of spots shot and the number of those evaluated. With this kind of information, we can compare strategies based on other parameters than the delivered dose, such as the speed of each one.

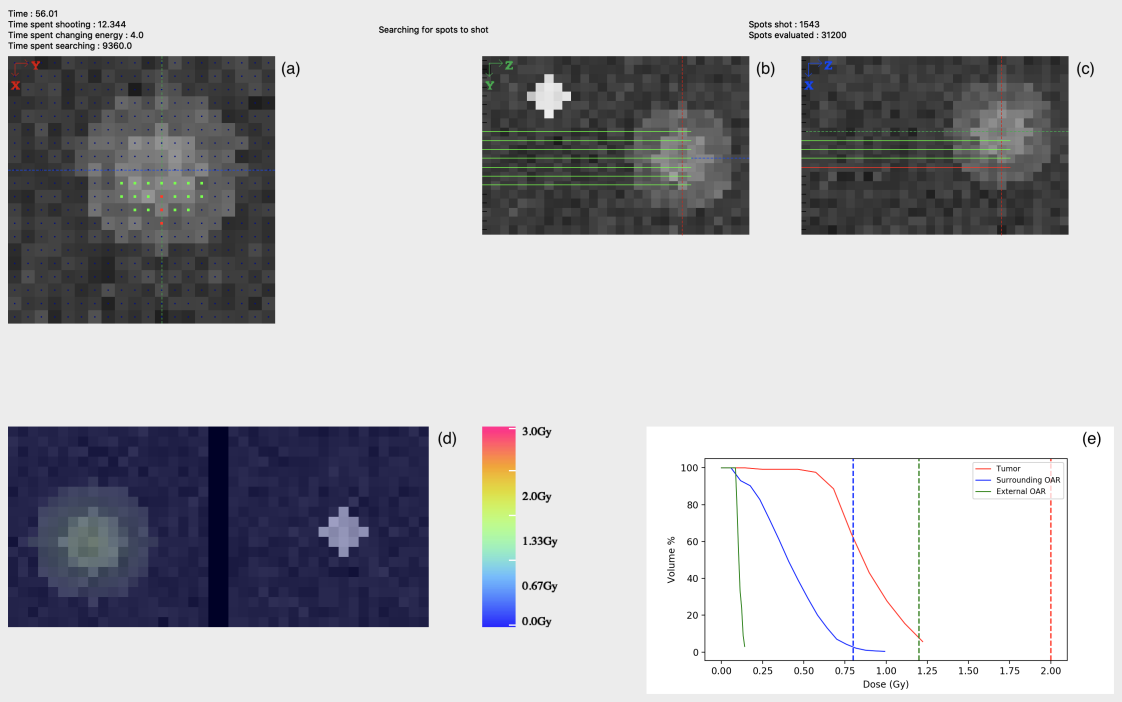

Figure 4.3: View of the Graphical User Interface. (a), (b) and (c): movement of the tumor in the 3 planes of space. Red points and lines mean that the beam was not shot while green points and lines mean that the beam was shot. (d): accumulated dose in the masks of the organs. (e): Dose-Volume Histogram.

4.1.4 Simulation tools

This simulation was carried out with the open-source programming language Python 3.7. All the results were obtained when running the simulation on a personal computer. This computer runs on macOS Mojave with a processor Intel Core i9 (2,4 GHz) and 16 Go of RAM.

4.2 Methods

Now that the main parameters of the simulation are defined, we can focus on the methods used in this work. We decided to divide this part in two. First, we will explain how our dose calculation was done. Then, we will discuss the different strategies developed to deliver the dose optimally in real-time.

4.2.1 Dose calculation algorithm

In order to compute the dose delivered in a voxel, we used the Continuous Slowing Down Approximation (CSDA) method. With this method, the energy lost by each particle in each voxel is computed using the following formula [7]:

$$\Delta E = \rho \cdot s \cdot SP(E)$$

Where: ΔE represents the difference in energy between two voxels, ρ is the mass density, s is the step length and SP the stopping power.

The density value depends on which organ the beam is going through. The step length is a fixed value and we consider it equal to the voxel size in the z-direction. The stopping power is the quantity of energy lost per unit of distance travelled. Databases of stopping power can be retrieved on PSTAR[1]. In those databases, there are the stopping powers of different materials for different energies. One has to interpolate the values given in the table of the correct material in order to retrieve the one corresponding to the current energy value of the beam. This energy variation is expressed in [MeV], so it is necessary to convert it into [Gy] in order to obtain the dose delivered within each voxel.

With this algorithm it is possible to obtain a dose profile as represented in Fig.4.4. Those plots show that a Bragg peak is obtained and that the delivered dose increases along with the depth in the tissue.

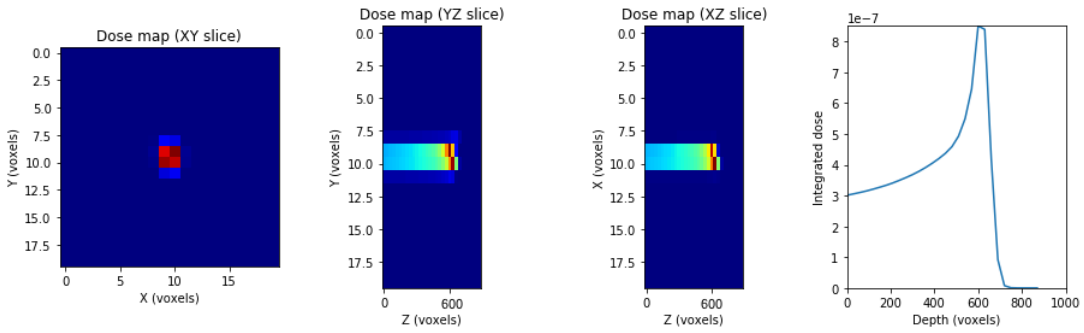

Figure 4.4: Different planes of the delivered dose with CSDA algorithm. To obtain this figure, we considered a beam composed of 2500 particles.

[1] https://physics.nist.gov/PhysRefData/Star/Text/PSTAR.html

The priority of this work was to have a rapid dose calculation method allowing to obtain a Bragg peak, the main characteristic of proton therapy. This is why, we chose this simplified but realistic method which can be computed quickly enough to consider the real-time aspect. We are aware that more advanced and accurate dose calculation methods exist but they take too long to allow the real-time decision making, and having the real value of the delivered dose was not our primary intention.

4.2.2 Real-time strategy

The real-time strategy is the main focus of this work. It is the key concept as it determines the way the dose is delivered in order to mitigate the effects of motion and interplay, and to obtain a dose as uniform as possible. In order to achieve this objective, the strategy identifies the optimal positions of the beam to be fired according to the dose already accumulated in the different organs.

Several strategies were considered. The aim here was to compare them and to determine which is better. 4 strategies were tested. Each was implemented in the same way, the only difference was the way of selecting the optimal beam positions to deliver the dose uniformly. In this section, we will explain the concept of real-time strategy, how it works and the differences between each strategy.

General implementation

The general implementation of the real-time strategies can be divided into 4 main steps repeated throughout the treatment fraction. These steps are as follows and will be explained in detail below:

1. Control of the Bragg peak position.
2. Selection of potential beams.
3. Evaluation of potential beams based on dose constraints.
4. Shot the spots where dose constraints are respected.

The first step of the algorithm is the **control of the Bragg peak position**. At the beginning of the treatment, the algorithm ensures that the Bragg peak occurs in the posterior portion of the tumor. To that end, the length of the tumor along the beam direction is divided into three identical segments. And, by simulating the firing of several beams around the volume of the tumor over several anatomies, it is possible to determine whether the initial beam energy makes it possible to have, initially, a dose delivered to the back of the tumor throughout the respiratory cycle. If needed, the beam mean energy is corrected to make sure that the dose is delivered at the back of the tumor.

In fact, this assessment is carried out throughout the whole treatment to take into account sudden changes in tumor position. In addition, when the mean dose in the posterior part of the tumor is equal to the prescribed dose, the beam energy is changed by decrements of around 25 MeV so that the Bragg peak now occurs in the anterior part of the tumor volume.

Fig.4.5 shows the result of this step. At the beginning of the treatment, when the energy has not been modified yet, the Bragg peak occurs outside the tumor volume (Fig.4.5a). On the other hand, as shown on Fig.4.5b, the Bragg peak is located at the back of the tumor after the correction of the beam mean energy.

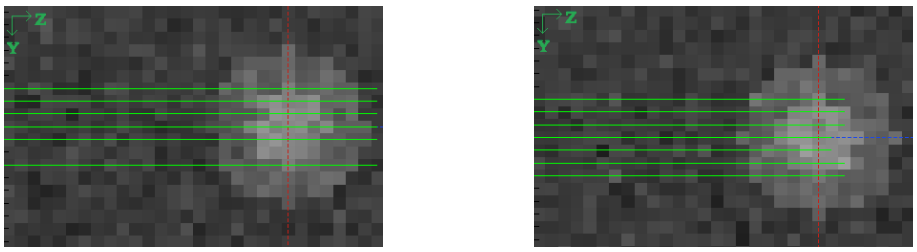

(a) Before (b) After

Figure 4.5: Positions of the Bragg peak (a) before and (b) after ensuring it occurs within the tumor volume.

After verifying that the Bragg peak position is within the tumor, the algorithm will **select 20 potential beams**, we call this set of 20 beams S_{pb}. This means that it determines the 20 optimal positions to deliver the dose in order to obtain a dose as close as possible to the objective. This objective dose corresponds to a dose of 2 Gy everywhere inside the tumor volume and no dose anywhere else. As mentioned above, each of the implemented strategies has its own way of determining the best beams. This will be explained in further detail in 4.2.2-Characteristics of the different strategies.

In the third step of the algorithm, **each beam of S_{pb} is evaluated based on the dose constraints** in order to decide whether this spot is to be fired or not. To that end, the algorithm checks whether the constraints on the dose at the specific beam position are met or not. This reasoning is done for the constraints on the organs at risk as well as on the tumor. This step divides the S_{pb} set in two groups: S_{sb} and S_{nsb}, respectively composed of the beams at positions where all the constraints are met and the beams at positions where at least one constraint is not respected.

Then, in the last step of the algorithm, **the spot is shot if every constraint at that position is respected**. This means that the beams of the S_{sb} set are fired while those of the S_{nsb} are not. Indeed, to limit excessive toxicity, it is necessary to stop delivering dose if it is already higher than the prescribed one. For this reason, the spot is not shot if the dose at that position is above the allowed dose in the different structures or over the mean dose in the tumor volume at that time.

Fig.4.6 highlights the S_{sb} and S_{nsb} sets. The beams belonging to S_{sb} are shown in green, which means that they are shot, whereas the beams belonging to S_{nsb} are colored in red so are not shot. The union of these two groups forms the S_{pb} set, composed of the 20 selected beams by the real-time strategy.

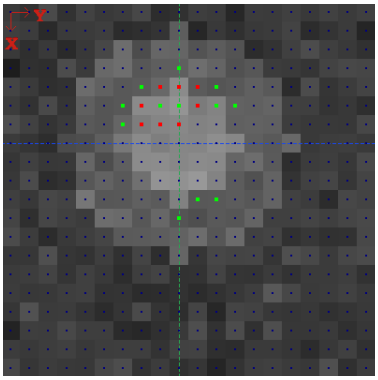

Figure 4.6: Visualization of the different sets of beams. S_{sb} is represented in green and S_{nsb} in red. The union of both is the S_{pb} set.

Finally, these different strategies stop and **the treatment fraction is deemed complete** when the mean dose within the tumor volume is equal to the prescribed dose, i.e. 2 Gy in this work.

Characteristics of the different strategies

In this part of the work, we will introduce the characteristics of each of our strategies and their differences.

The first strategy, **FIxed BEam SCanning MOtion (FIBESCMO)**, is largely inspired by what is done today in proton therapy. The beam follows a predefined scanning motion across the entire grid. If the position of the beam is not within the safety margin around the tumor, the beam will not be selected and the scanning motion continues. Otherwise, if the beam is within the security zone, the beam will be selected. In this case, the position will then be evaluated, as described in the previous section, to determine whether the beam is to be shot or not. Fig.4.7 displays the flow chart of this strategy.

The main disadvantage of the FIBESCMO strategy is the predefined beam scanning motion. Indeed, during certain anatomies, the positions of the beam are not in the security margins, so they are not shot. It can last a long time, hence the waste of time. The other strategies developed in this work counter this waste of time. These new strategies aim the beam directly to the volume of the tumor as they no longer consider a scanning movement of the beam.

The second strategy, **FIrst TWenty SAtisfying COnstraints (FITWSACO)**, is the simplest of all. The implementation of this strategy is different from the general implementation. In this case, for each new anatomy, the algorithm selects the first 20 spots of the tumor that respect the different dose constraints. Fig.4.8 displays the flow chart of this strategy.

The FITWSACO strategy has one major flaw. During a large part of the treatment, it always selects the same beam positions, since the constraints can be met while shooting at those positions. Therefore, the dose is always delivered in the same locations. The next strategies will improve this shortcoming via a dose-based beam selection.

The third strategy, **MInimum ACcumulated DOse (MIACDO)**, selects beam positions based on the dose already accumulated in the tumor. For each position of the projected tumor plane, the sum of the accumulated dose within each tumor voxel along the beam direction at that position is calculated. The positions are then sorted in ascending order. The algorithm selects the first 20 beam positions, namely those with the smallest sums. From then on, the algorithm checks if the constraints are met before shooting. Fig.4.9 displays the flow chart of this strategy.

The fourth strategy, **COmpute GAin (COGA)**, uses another method to optimize the beam selection. This method includes the evaluation of a gain for each position of the projected tumor plane extended by one voxel. We noted that the edges of the tumor were less reach which led us to enlarge the shooting zone. To calculate the gain, a fictitious shot is taken. This strategy pretends to fire a beamlet at that position and takes into account the dose delivered by this false shot to compute the gain.

In fact, this strategy can itself be divided into several strategies. Three different ways of calculating the gain were implemented to obtain the most uniform dose possible.

1. The first one is **COmpute GAin ONe POsition DOse (COGA_ONPODO)**. In this strategy, the gain is defined by the following formula:

$$\text{Gain}_{xy} = \left(\sum_i \text{Objective dose[x,y,i]} - \left(\sum_i \text{Accumulated dose[x,y,i]} + \sum_i \text{Current dose[x,y,i]} \right) \right)^2$$

   Where:

   - Gain_{xy} is the gain at the position (x,y) of the extended tumor projected plane.
   - i is the index of the voxels along the beam direction at position (x,y).
   - Objective dose[x,y,i] is the vector of the voxels along the beam direction at position (x,y) of the 3D objective dose map, defined by a dose equal to 2 Gy in the tumor volume and no dose anywhere else.
   - Accumulated dose[x,y,i] is the vector of the voxels along the beam direction at position (x,y) of the 3D accumulated dose map. It represents the accumulated dose from previous anatomies in the tumor but also in the two organs at risk.
   - Current dose[x,y,i] is the vector of the voxels along the beam direction at position (x,y) of the 3D current dose map. Current dose represents the dose that would be delivered if the shot was fired from that position. In this case, it is important to transform the current dose in the reference anatomy, so that the dose delivered at the current anatomy is added to the corresponding volume and not elsewhere.

   It is important to note that this strategy computes the gain solely based on the dose delivered at the position (x,y) of the extended projected tumor plane, it does not take into account the dose delivered in neighbouring voxels.

2. The second one is **COmpute GAin TUmor VOlume DOse (COGA_TUVODO)**. In this case, the gain is equal to the Mean Squared Error (MSE) and is defined by:

$$\text{Gain}_{xy} = \text{MSE} = \frac{1}{n}\sum_{i=1}^{n}(Y_i - \hat{Y}_i)^2 = \frac{1}{n}\sum_{i=1}^{n}(\text{Objective dose}_i - \text{Cumulative dose}_i)^2$$

Where:

- Gain_{xy} is the gain at the position (x,y) of the extended tumor projected plane.
- i is the index of the voxels in the tumor.
- Y_i stands for the truth target values. In this work, we consider this to be the objective dose limited to the tumor mask. This means that it is a 3D dose map, of the tumor shape, with a dose equal to 2 Gy in each voxel.
- $\hat{Y}_i$ stands for the predicted values. In this work, we consider this to be the cumulative dose, which is the sum of the accumulated dose from previous anatomies and the current dose that would be delivered if the shot was fired from the position (x,y). Cumulative dose is also limited to the tumor mask.

It is interesting to note that this strategy is based on the dose within the entire tumor volume but does not consider the delivered dose in the OARs.

3. The last one is **COmpute GAin TUmor COnstraints (COGA_TUCO)**. This strategy computes the gain using an objective function. The objective function is a sum of multiple objectives and can be defined by the following formula:

$$\text{Gain}_{xy} = f(d) = \sum_i w_i \cdot (\text{Cumulative dose} - \text{Constraint}_i)$$

Where:

- Gain_{xy} is the gain at the position (x,y) of the extended tumor projected plane.
- i is the index of each objective.
- w_i represents a weight. Each objective is multiplied by a weight which is higher or lower according to its priority.
- Cumulative dose is the sum of the accumulated dose from previous anatomies and the current dose that would be delivered if the shot was fired from the position (x,y). Depending on the objective, a particular value of this dose will be chosen.
- Constraint_i stands for the multiple constraints used to obtain a dose as close to the objective as possible.

In this work, we only used tumor objectives. For that purpose, we slightly adjusted the tumor constraint $D_{mean} = 2$ Gy in order to have constraints on the maximum dose and the minimum one. This gives us the following formula:

$$\begin{aligned}\text{Gain}_{xy} = f(d) = \quad & 10 \cdot \Big(max(\text{Cumulative dose}) - 1.05 \cdot (\text{Tumor constraint})\Big)^2 \\ & + 2 \cdot \Big(min(\text{Cumulative dose}) - 0.95 \cdot (\text{Tumor constraint})\Big)^2 \\ & + 3 \cdot \Big(mean(\text{Cumulative dose}) - \text{Tumor constraint}\Big)^2\end{aligned}$$

In order to have a steep slope in the tumor's Dose-Volume Histogram, we chose to put a large weight on the maximum constraint to minimize the maximum delivered dose within the tumor.

The beams that are selected in the three COGA strategies are the 20 positions with the smallest gains. Once the optimal positions are determined, the algorithm evaluates, according to the constraints, whether these beams will be shot or not. Fig.4.10 displays the flow charts of this strategy.

As already said, Fig.4.7, Fig.4.8, Fig.4.9 and Fig.4.10 display the flow chart of respectively the FIBESCMO strategy, the FITWSACO strategy, the MIACDO strategy and the COGA strategy. These figures show that the general implementation is the same for every strategy and that each strategy differs from the others in the way it determines the optimal beams to obtain a dose close to the ideal case.

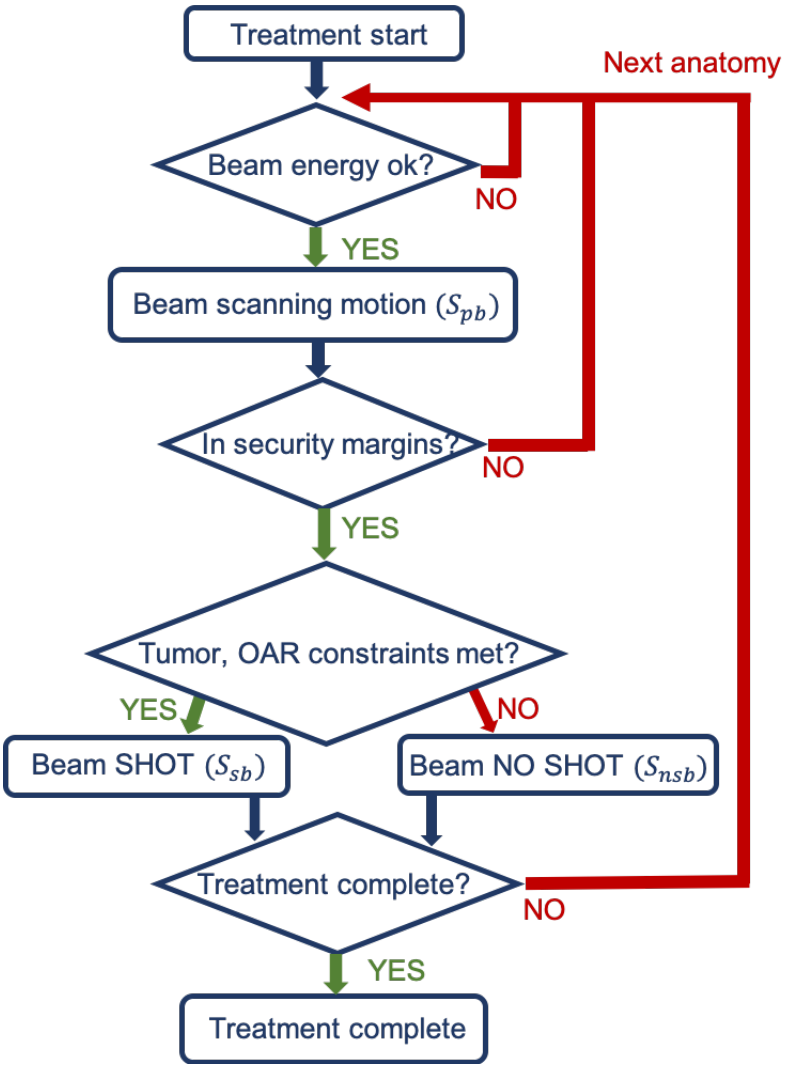

Figure 4.7: Flow chart scheme of the FIBESCMO strategy. The particularity of this strategy is that it uses a fixed beam scanning motion.

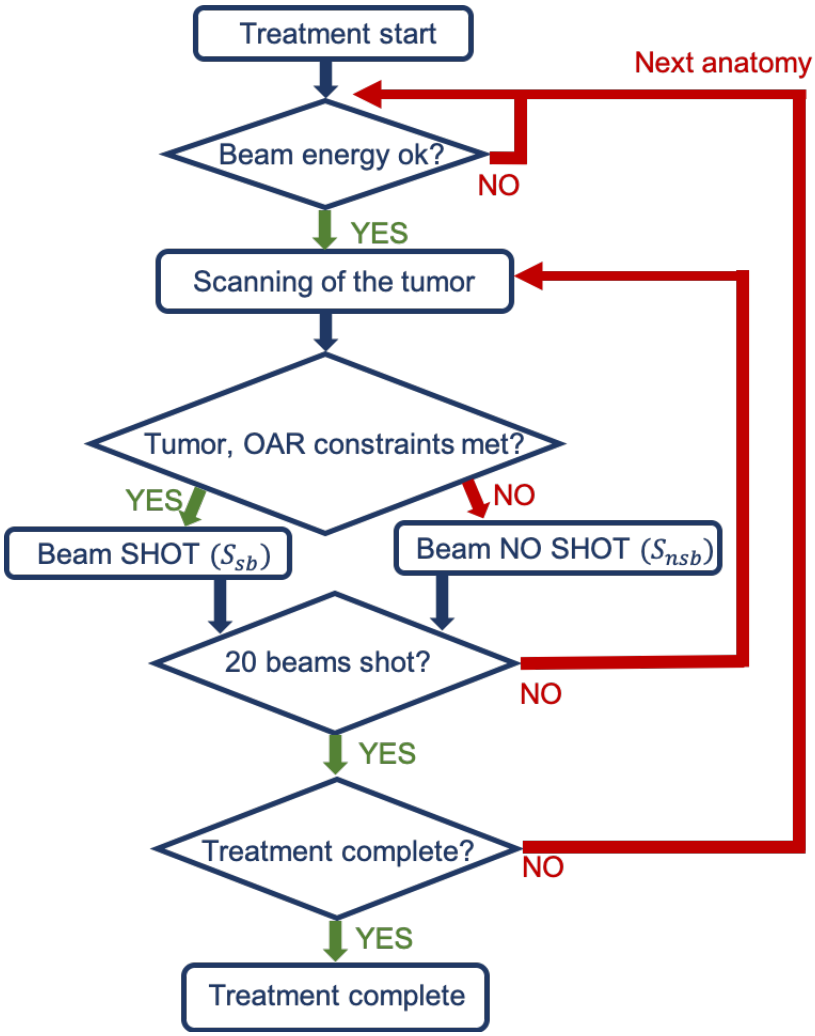

Figure 4.8: Flow chart scheme of the FITWSACO strategy. The particularity of this strategy is that the algorithm selects the first 20 spots satisfying the different dose constraints.

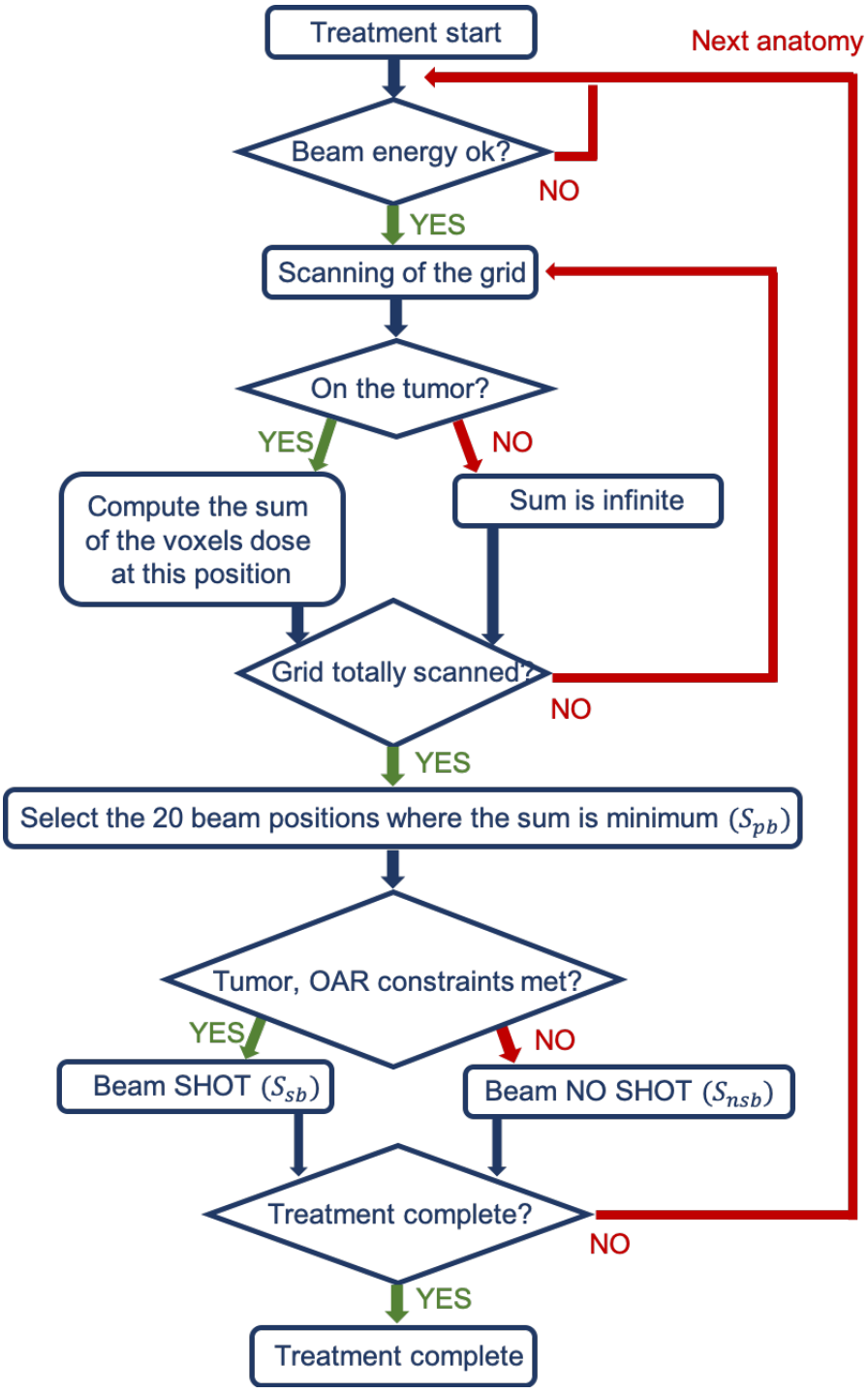

Figure 4.9: Flow chart scheme of the MIACDO strategy. This strategy computes the sum of the doses accumulated in the tumor voxels at each position and selects the minimum.

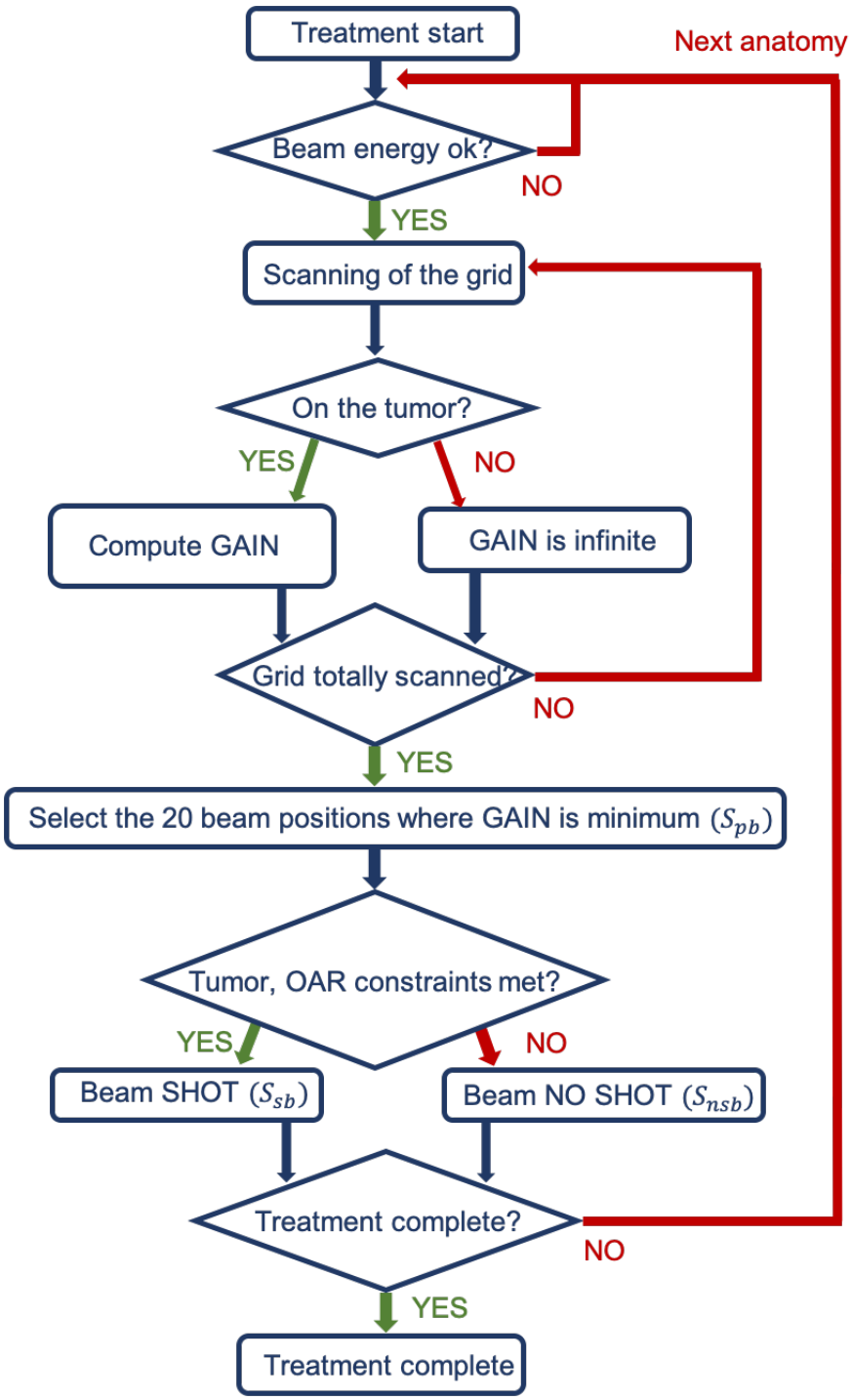

Figure 4.10: Flow chart scheme of the COGA strategy. This strategy evaluates a gain by pretending to shoot at each position of the projected tumor plane.

4.3 Results and discussion

Now that the implementation of the real-time strategies is fully understood, let's take a look at the results. We decided to divide this part in three. First, we will compare the general appearance of our results from the ones in the literature. Then, we will perform a specific analysis to compare the results obtained with the 6 real-time strategies. Finally, we will analyse the robustness of one strategy in particular.

4.3.1 Overall analysis

Before diving into the details of our results, it could be interesting to compare the general appearance of the results obtained with our approach from the ones in the literature.

A theoretical dose distribution and a typical Dose-Volume Histogram (DVH) of the lung plans are shown in Fig.4.11 when using proton therapy. Those are obtained after the optimization step in the clinical workflow. These two figures show that the delivered dose within the tumor volume is equal to the prescribed dose whereas it is almost null in the neighbouring organs. This is noticeable on the dose distribution in Fig.4.11a where the dose delivered within the tumor is red, representing a dose of 60 Gy. This figure shows that the further the delivered dose is from the target volume, the lower it becomes. In the DVH represented in Fig.4.11b, this phenomenon can also be noted. More than 90% of the tumor volume receives the prescribed dose while the neighbouring organs at risk receive a very low dose in their entire volumes and only a limited part of them receive a higher dose.

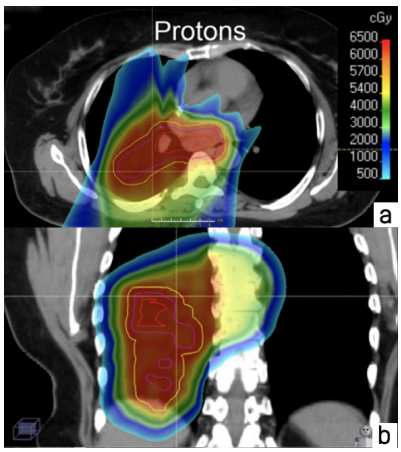

(a) Typical dose distribution represented for (a) transversal and (b) coronal views [39].

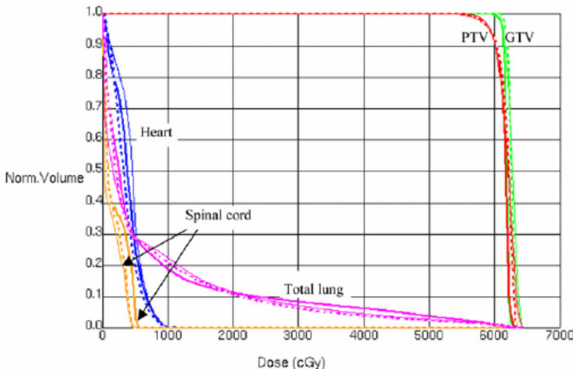

(b) Typical Dose-Volume Histogram [17].

Figure 4.11: Typical dose distribution and Dose-Volume Histogram obtained for lung treatment with a prescribed dose of 60Gy.

The dose distributions and DVHs obtained when running our simulation are shown in Fig.4.12. This figure displays one example of the results obtained with each real-time strategy at the end of the treatment, i.e. when the mean delivered dose within the tumor is equal to the prescribed dose. As shown in this figure, the general appearance of our results are similar to those in the literature. For each strategy, the highest delivered dose is in the tumor and decreases the further we get from the target.

At first glance, the results of the different strategies appear to be similar. However, if we look at them a more closely, we can notice some differences. Depending on the strategy, the red curve (representing the dose within the tumor) may have a more or less vertical slope, the green curve (representing the dose within the external OAR) may be more or less to the right,... These first observations will be reviewed in detail in the following analyses in order to highlight the strengths and weaknesses of each strategy.

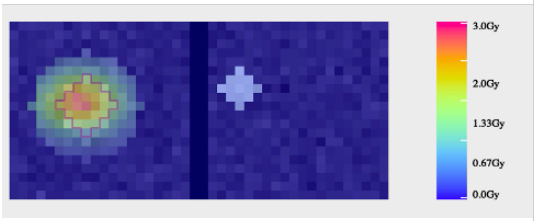

(a) Dose distribution of FIBESCMO strategy

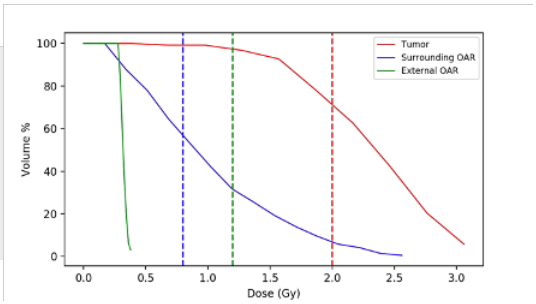

(b) DVH of FIBESCMO strategy

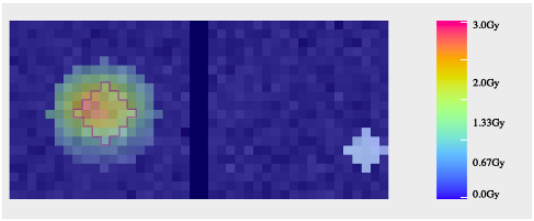

(c) Dose distribution of FITWSACO strategy

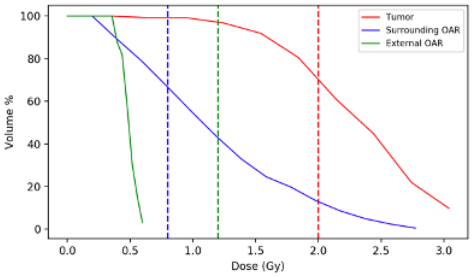

(d) DVH of FITWSACO strategy

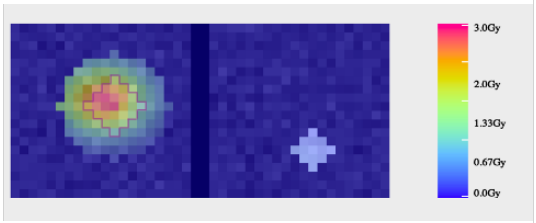

(e) Dose distribution of MIACDO strategy

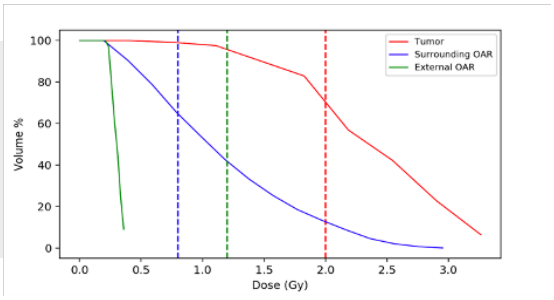

(f) DVH of MIACDO strategy

Figure 4.12: Dose distribution (left column) and DVH (right column) obtained with the real-time approaches. The dose distribution figures show the dose delivered in the plane passing through the center of each structure. On its left, the dose in the surrounding OAR and in the tumor (contour in purple). On the right, the dose in the external OAR. The dose distribution figures are accompanied by a color bar allowing to visualize the dose delivered within a voxel. The DVH figures show the dose delivered within the tumor (red), the surrounding OAR (blue) and the external OAR (green). The dotted lines show the constraints applied on each of those organs. - part 1

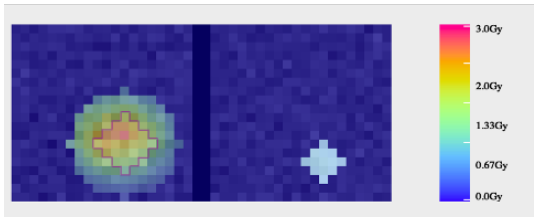

(a) Dose distribution of COGA_ONPODO strategy

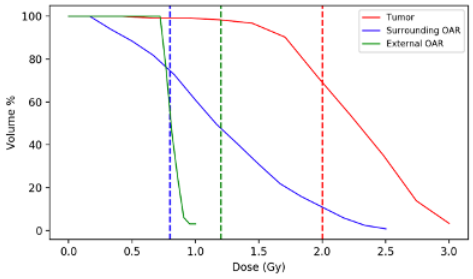

(b) DVH of COGA_ONPODO strategy

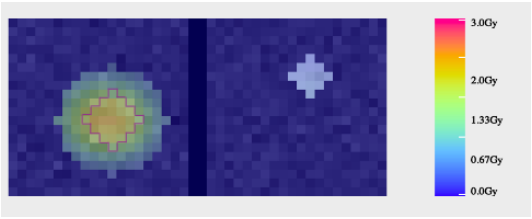

(c) Dose distribution of COGA_TUVODO strategy

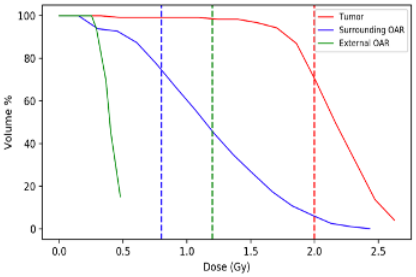

(d) DVH of COGA_TUVODO strategy

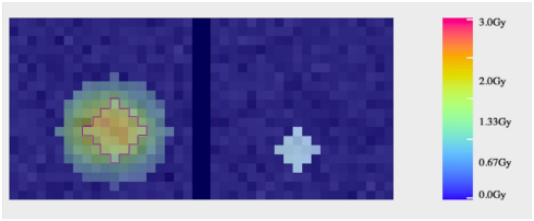

(e) Dose distribution of COGA_TUCO strategy

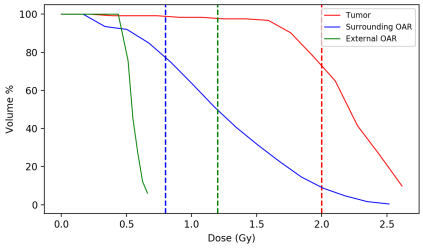

(f) DVH of COGA_TUCO strategy

Figure 4.12: Dose distribution (left column) and DVH (right column) obtained with the real-time approaches. The dose distribution figures show the dose delivered in the plane passing through the center of each structure. On its left, the dose in the surrounding OAR and in the tumor (contour in purple). On the right, the dose in the external OAR. The dose distribution figures are accompanied by a color bar allowing to visualize the dose delivered within a voxel. The DVH figures show the dose delivered within the tumor (red), the surrounding OAR (blue) and the external OAR (green). The dotted lines show the constraints applied on each of those organs. - part 2

4.3.2 Specific analysis

Comparative analysis of real-time strategies

We will now analyze more specifically the performance of the various strategies implemented. Therefore, we must define several comparison criteria in order to assess the obtained results. We grouped these metrics according to different axes of analysis. Table 4.5 summarizes those metrics.

Table 4.5: Metrics and the corresponding axis of analysis, used in the comparative analysis of real-time strategies.

Metric	Axis of analysis
Minimum dose in the tumor	Intratumoral dose quantity
$D_{95\%}$ in the tumor	Intratumoral dose quantity
Maximum dose in the tumor	Intratumoral dose quantity
$D_{5\%}$ in the tumor	Intratumoral dose quantity
V_{2Gy} in the tumor	Intratumoral dose quantity
Standard deviation	Intratumoral dose homogeneity
Homogeneity Index	Intratumoral dose homogeneity
Mean dose in the surrounding OAR	Extratumoral dose quantity
Mean dose in the external OAR	Extratumoral dose quantity

To get the results of this section, we executed the simulation 15 times for each strategy. As shown in Appendix A.2, this number of simulations is sufficient to have convergence of the mean of the metrics.

Moreover, it should be noted that the comparison with results stemming from a more basic strategy, namely continuous shooting, a strategy used currently, was not performed. Indeed, had we used this approach, the results would have been worse than what they really are since there were no optimization step.

The first metric is the **minimum dose** within the tumor. This metric evaluates the minimum dose of the voxels in the structure. This metric is important to study because it makes it possible to evaluate if all voxels receive a dose close to the prescribed one.

The second metric is the $\mathbf{D}_{95\%}$ within the tumor, it evaluates the minimum dose delivered to 95% of the target volume. In fact, this metric is more commonly used to evaluate the minimum delivered dose within a structure since it eliminates outliers. It is possible that a voxel is not properly reached by the beam because of its depth or even its relative position to the external OAR. But, this voxel is an exception. To compute the value of $D_{95\%}$, we based ourselves upon the DVH. Since it does not always return exactly the dose delivered in 95% of the tumor volume, we performed a linear interpolation between the two surrounding data to obtain exactly the dose delivered at this tumor volume percentage.

Fig.4.13 shows the results obtained for these two metrics. It can be directly observed that the minimum dose delivered within the tumor is very low for each strategy, ranging from 0 to 0.2 Gy. On the other hand, the $D_{95\%}$ is much higher and is close to the prescribed dose value, confirming the interest of working with this metric. For this criterion, the two strategies COGA_TUVODO and COGA_TUCO give the best results. In those cases, the medians are equal to 1.5389 Gy and 1.5289 Gy whereas for the FITWSACO strategy, which is the least optimal here, the median is 1.2987 Gy.

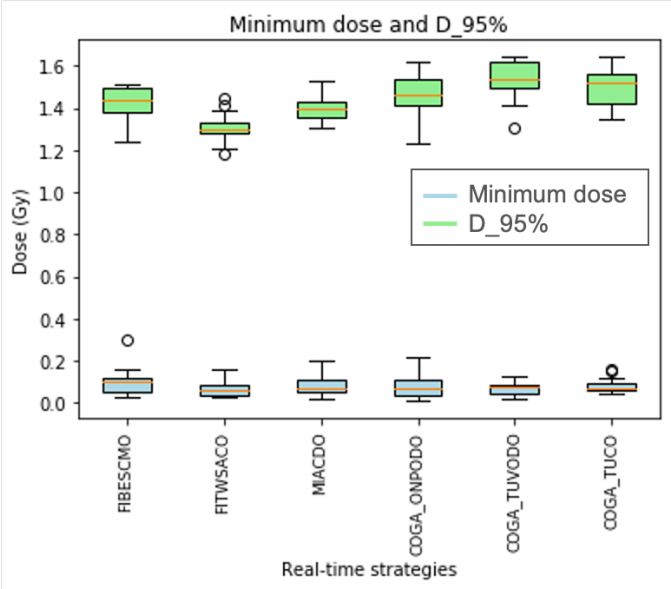

Figure 4.13: Boxplot of the minimum dose (blue) and $D_{95\%}$ (green) delivered within the tumor for each real-time strategy. The orange line represents the median and the edges of the box indicate the 25th and 75th percentile.

The third metric evaluates the **maximum dose** delivered within the tumor volume. To have a uniform dose within the target, it is necessary for the maximum dose to be equal to the prescribed dose or even slightly higher.

The fourth metric is the $\mathbf{D}_{5\%}$ in the tumor, it evaluates the maximum delivered dose to 5% of the tumor volume. Here again, it is recommended to use this metric to eliminate exceptions. It is possible that the maximum delivered dose is only hitting one voxel of the tumor, which is a small percentage of its volume. To compute the value of $D_{5\%}$, we performed a linear interpolation between the two surrounding data in the DVH to obtain exactly the dose delivered at this tumor volume percentage.

In contrast to the minimum metrics, the difference between the maximum dose and $D_{5\%}$ is way less pronounced. As shown in Fig.4.14, the boxplots of these two metrics overlap. This means that the maximum dose within the tumor is generally delivered in more than 5% of its volume. We can see that the three COGA strategies give similar results. In those cases, the value of the maximum delivered dose is between 2.7 and 3 Gy. On the other hand, the other three strategies almost always have a maximum dose higher than 3 Gy. In addition, for those three strategies, the distribution intervals are wider which means that they are more unstable than the three best ones.

It can be observed that this analysis divides the 6 real-time strategies into two distinct groups, those whose maximum is relatively small (the three COGA strategies) and the others (FIBESCMO, FITWSACO and MIACDO). Therefore, let's take a closer look to see if this dichotomy is confirmed with the other metrics.

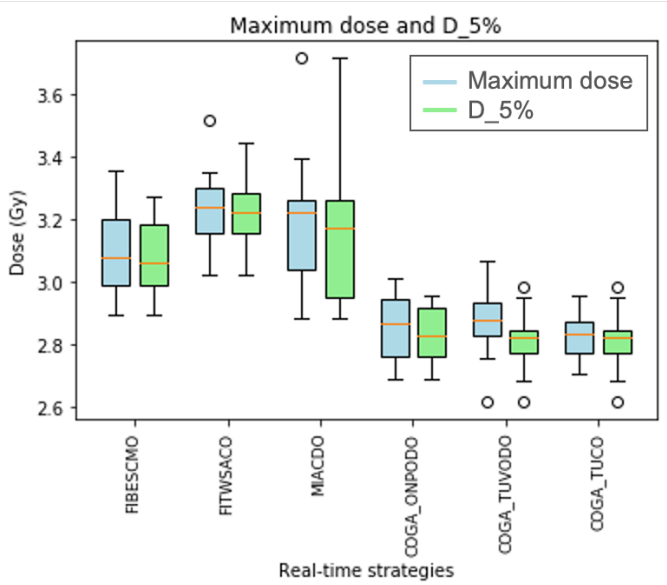

Figure 4.14: Boxplot of the maximum dose (blue) and $D_{5\%}$ (green) delivered within the tumor for each real-time strategy. The orange line represents the median and the edges of the box indicate the 25th and 75th percentile. The circle shows an outlier.

The fifth metric is $\mathbf{V}_{2Gy}$ which corresponds to the percentage of the tumor volume receiving a dose greater than or equal to the prescribed dose. In the ideal case, 100% of the tumor should receive a dose equal to its prescription. This is why, in this work, we tried to maximize this volume.

Fig.4.15 highlights the results obtained for each strategy when evaluating the V_{2Gy} metric. We can observe that the median is the highest in the COGA_TUCO strategy. In this case, the median value of V_{2Gy} is 71.95% and we can observe that it drops below 70% once, it is an outlier. On the other hand, the median of the worst strategy, FITWSACO, is equal to 69.84%. Moreover, the distribution interval for this metric is around 4% of the tumor volume for all strategies.

In Fig.4.15, we can see that the separation highlighted in the previous metric is still present but less pronounced.

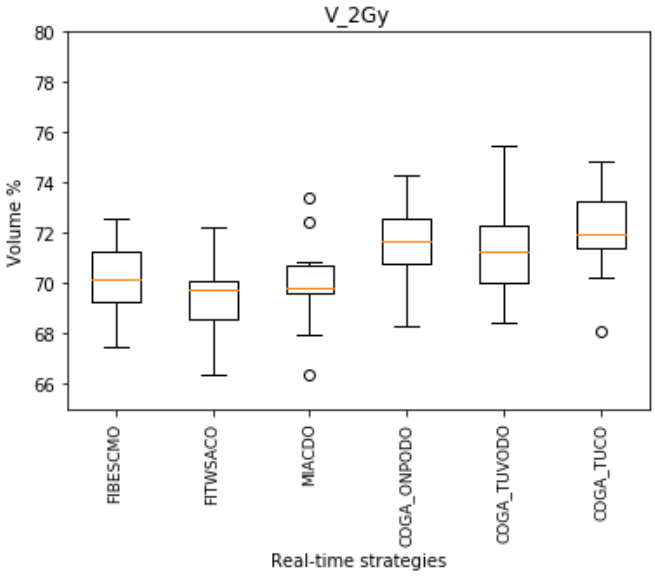

Figure 4.15: Boxplot of the V_{2Gy} metric for each real-time strategy. The orange line represents the median and the edges of the box indicate the 25th and 75th percentile. The circles show outliers.

The second axis of analysis is the homogeneity of the delivered dose within the tumor. This is why, the sixth metric analyses the **standard deviation** of the delivered dose within the tumor structure. It is interesting to study the standard deviation as it can measure the dispersion of the delivered dose within tumor voxels. We want a minimum standard deviation to ensure a homogeneous dose in the tumor.

For this metric, as shown in Fig.4.16, the best strategy is the COGA_TUCO one since it has the lowest median (0.4067 Gy). The gain between this strategy and the worst one, FITWSACO, is equal to 36.23%. Moreover, it can be noticed that the distribution interval of the COGA_TUCO strategy is the smallest, which shows a certain stability. It is around 0.08 Gy, whereas in the case of the MIACDO strategy it is around 0.2 Gy.

This figure also highlights the dichotomy presented above. It can be seen that the FIBESCMO, FITWSACO and MIACDO strategies, which had a higher maximum dose, have a higher standard deviation while the standard deviation is reduced for the three COGA strategies which had a lower maximum dose.

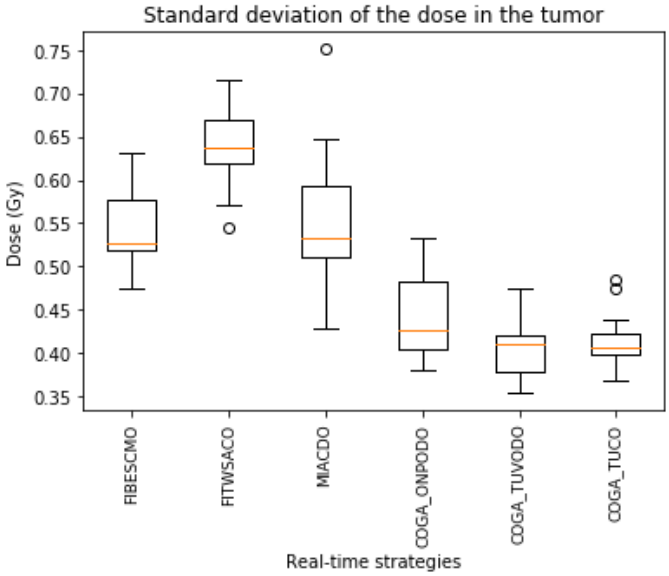

Figure 4.16: Boxplot of the standard deviation of the dose delivered within the tumor for each real-time strategy. The orange line represents the median and the edges of the box indicate the 25th and 75th percentile. The circles show outliers.

The seventh metric is the **Homogeneity Index (HI)**. It is an objective tool to analyze the uniformity of the dose distribution in the target volume. In this work, we consider the homogeneity index defined by the following formula:

$$\frac{D_{5\%} - D_{95\%}}{D_p}$$

In this formula, $D_{95\%}$ and $D_{5\%}$ are the minimum and maximum dose delivered to, respectively, 95% and 5% of the target volume and D_p is the prescribed dose. This formula takes into account $D_{95\%}$ and $D_{5\%}$ to represent the minimum and maximum dose because, as already said, the true minimum or maximum dose is unreliable since their values rely heavily on the dose computation parameters. The homogeneity index indicates the ratio between the maximum and minimum dose in the target volume. A lower value indicates a more homogeneous dose distribution in the volume [40].

The homogeneity index should be close to 0 to ensure that the dose delivered within the tumor is homogeneous. We therefore wish to obtain a low value of this metric with the optimal strategy. In Fig.4.17, we can see that the COGA_TUCO strategy gives the best result and has its median equal to 0.6388. Moreover, in the case of this strategy, the distribution interval is narrow, meaning that it is quite stable. On the contrary, the FITWSACO strategy gives the worst result with an HI ranging from 0.85 to 1.1 and a median equal to 0.9546. This means that the COGA_TUCO strategy gives a gain of 33.07% in terms of homogeneity index compared to the FITWSACO strategy.

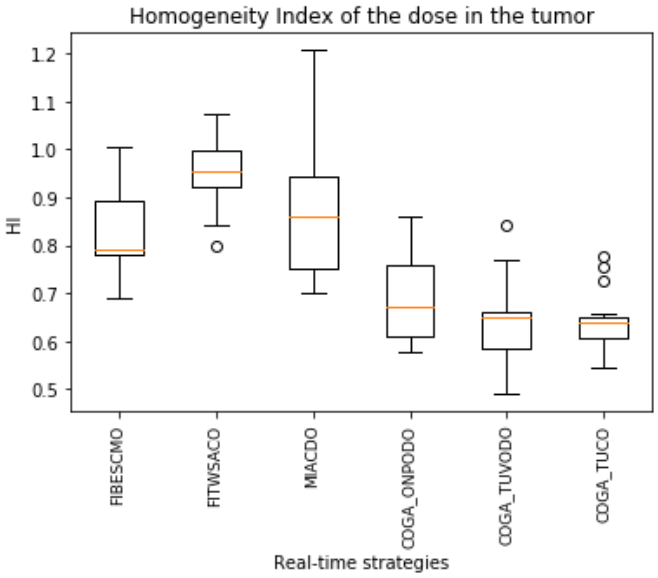

Figure 4.17: Boxplot of the homogeneity index of the tumor dose for each real-time strategy. The orange line represents the median and the edges of the box indicate the 25th and 75th percentile. The circles show outliers.

The third axis of analysis is the extratumoral dose quantity since one of the objectives of this work is to avoid delivering dose to neighbouring organs. This is why, the eighth and ninth metrics evaluate the **mean delivered dose in the neighbouring organs**. In this work, we considered that the surrounding OAR is a lung while the external one is the heart.

As already said, in the case of the surrounding OAR, we consider a specific constraint of the lung, $D_{mean} < 0.8$ Gy. As shown in Fig.4.18a, this constraint is never respected as the mean dose in this structure is always above 0.8 Gy. We can see that the mean delivered dose within this organ is lower when the FIBESCMO strategy is used. In this case, the value varies slightly around 0.82 Gy. On the other hand, when the other strategies are used, the mean delivered dose within the surrounding OAR is greater and varies around 1 Gy. Since this constraint is never respected, we wanted to study the percentage of its volume receiving a dose of 0.8 Gy to see if the same observations were possible. The answer to this question is shown in Fig.4.18b. In this case, we can do the same analysis as before. For the FIBESCMO strategy, $V_{0.8Gy}$ is lower than for the other strategies with a median of 56.2052% while, for the three COGA strategies, the medians are around 74%.

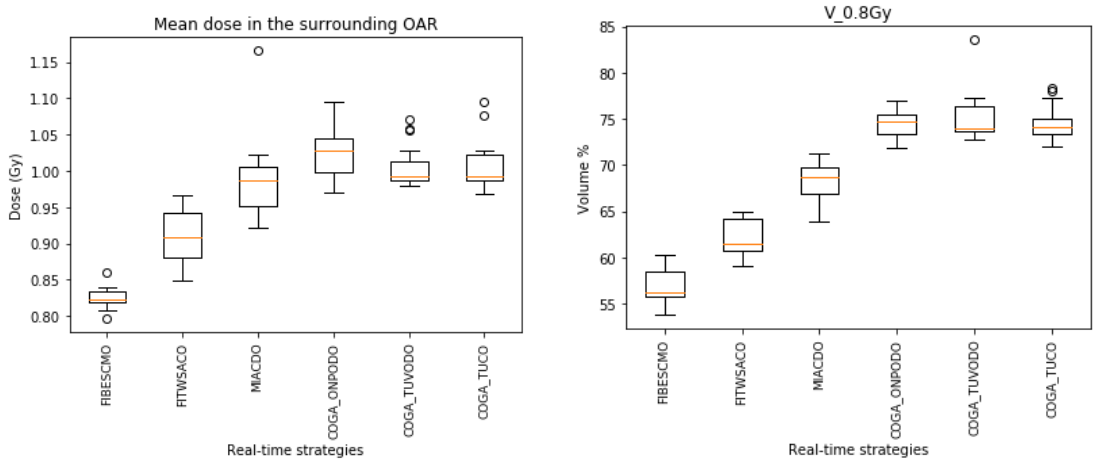

(a) Mean dose

(b) $V_{0.8Gy}$

Figure 4.18: Boxplot of the mean dose delivered within the surrounding OAR and boxplot of the $V_{0.8Gy}$ metric for each real-time strategy. The orange line represents the median and the edges of the box indicate the 25th and 75th percentile. The circles show outliers.

In the literature, the constraints used for the heart are that the dose received by a certain percentage of the volume must not exceed a certain value. In this work, we considered a simplified constraint which is $D_{mean} < 1.2$ Gy. The results obtained for this organ are valid for each strategy. Fig.4.19 shows that the mean dose in this organ is always lower than the one imposed by the constraint. This figure also shows that only the COGA_TUCO strategy seems to be stable according to this metric. The interval in which the mean dose varies is much smaller than the one of the other strategies. For this strategy the mean dose in the external OAR ranges from 0.3 to 0.5 Gy with some outliers, while it can vary from 0.1 to 0.9 Gy for the MIACDO strategy.

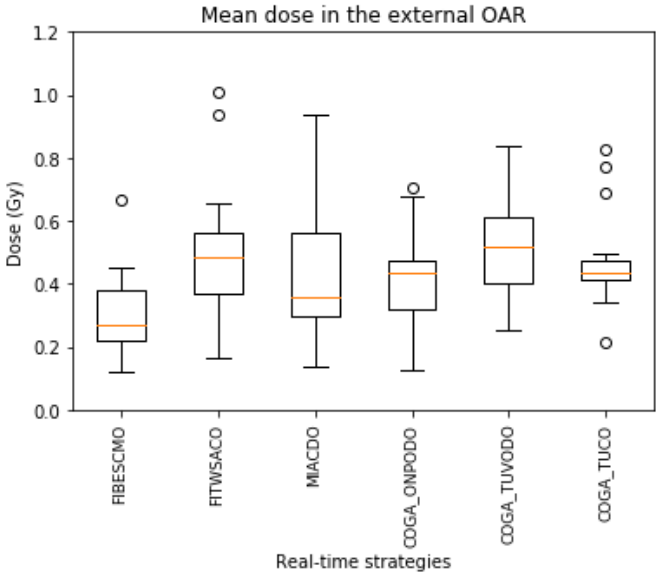

Figure 4.19: Boxplot of the mean dose delivered within the external OAR for each real-time strategy. The orange line represents the median and the edges of the box indicate the 25th and 75th percentile. The circles show outliers.

In-depth analysis of each real-time strategy

These different analyses made it possible to compare the results obtained with each real-time strategy. We quickly noticed the formation of two distinct groups within the 6 implemented strategies. We are now going to perform an in-depth analysis of each one based on the results of the above analyses, and we will try to understand why are these results the ones obtained.

The first strategy is **FIBESCMO**. Table 4.6 summarizes the results obtained with this real-time strategy for the most relevant metrics.

Table 4.6: Values of the median of the different metrics obtained with the FIBESCMO strategy and the ideal value of each obtained after 10 simulations.

	$D_{95\%}$ [Gy]	$D_{5\%}$ [Gy]	V_{2Gy} [%]	HI	D_{mean} in surr. OAR [Gy]	D_{mean} in ext. OAR [Gy]
FIBESCMO strategy	1.4389	3.0623	70.1664	0.7926	0.8224	0.2721
Ideal case	2	2	100	0	< 0.8	< 1.2

As a reminder, this strategy considers a fixed beam scanning motion and the beam is shot when its position is within the security margins around the tumor and if all the constraints are met. We observe that this strategy gives quite good results in relation to the delivered dose within the tumor. The homogeneity index stays below 1, with a median of 0.7926 as shown in Table 4.6. Moreover, it can be noted that the results obtained with this strategy for each metric vary a lot. One of the possible reasons for this observation is the noise around the tumor position. This noise is generated by the respiratory motion. Therefore, the position can never be the same between two simulations. As the firing pattern of this strategy is determined by the synchronization between the tumor position and the beam scanning motion, which does not take into account the different tumor positions, the firing pattern deeply varies from one simulation to the other, generating quite different results. The simulation time for this strategies is also much longer than for the others since the beam is outside the target area during a large part of the treatment.

We can also observe that the algorithm implemented in this strategy to meet the constraints on neighbouring organs at risk fulfills its task because the mean delivered dose within those organs remains low. The median of the mean delivered dose in the surrounding OAR is 0.8224 Gy, which is slightly above the constraint value and the median of the mean delivered dose in the external OAR is 0.2721 Gy, corresponding to 22.67% of the dose constraint.

The second strategy implemented is **FITWSACO**. Table 4.7 summarizes the results obtained with this real-time strategy for the most relevant metrics.

Table 4.7: Values of the median of the different metrics obtained with the FITWSACO strategy and the ideal value of each obtained after 15 simulations.

	$D_{95\%}$ [Gy]	$D_{5\%}$ [Gy]	V_{2Gy} [%]	HI	D_{mean} in surr. OAR [Gy]	D_{mean} in ext. OAR [Gy]
FITWSACO strategy	1.2987	3.2228	69.7647	0.9546	0.9091	0.4858
Ideal case	2	2	100	0	< 0.8	< 1.2

The above analyses show that this strategy is the least optimal. The analyses of the tumor criteria show that the dose delivered within the tumor is relatively heterogeneous, with a homogeneity index ranging from 0.85 to 1.1, and a median equal to 0.9546 as shown in Table 4.7. This is due to the fact that $D_{5\%}$ is very significant since it corresponds to more than 160% of the prescribed dose while $D_{95\%}$ remains low and is around 60% of the prescribed dose. This phenomenon could be explained by the implementation of this strategy. As it directly selects the beam positions satisfying the constraints, they stay the same during a large chunk of the treatment since the constraints still allow to shoot at this location. The dose is therefore delivered over a long period of time at the same location, resulting in a clear separation between the tumor volume receiving too high of a dose and the rest receiving too low of a dose. To minimize the gap between the maximum dose and the minimum one, it could be interesting to modify how the algorithm scans the tumor. In this work, we considered only a horizontal movement. However, the combination of different directions of motion and opposite starting points should enable the selection of different positions of the tumor projected plane.

On the other hand, we observe that this strategy is quite good to avoid delivering the dose to the surrounding organs. This strategy generates a low mean dose in the surrounding OAR. Furthermore, the analysis of the metric $V_{0.8Gy}$ shows that this strategy also gives the second best result in this case. Again, this observation can be explained by the algorithm of this strategy. Since the dose is mainly delivered in one region of the tumor, the surrounding OAR is only reached in this region.

The third strategy is **MIACDO**. The above results show that it is an average strategy. Table 4.8 summarizes the results obtained with this real-time strategy for the most relevant metrics.

Table 4.8: Values of the median of the different metrics obtained with the MIACDO strategy and the ideal value of each obtained after 15 simulations.

	$D_{95\%}$ [Gy]	$D_{5\%}$ [Gy]	V_{2Gy} [%]	HI	D_{mean} in surr. OAR [Gy]	D_{mean} in ext. OAR [Gy]
MIACDO strategy	1.3942	3.1724	69.842	0.8605	0.9861	0.3581
Ideal case	2	2	100	0	< 0.8	< 1.2

As displayed in Table 4.8, the results of this strategy are average. For each criterion, it lies between the two extremes. For example, the median of the maximum dose is equal to 3.1724 Gy while the one of the minimum dose is 1.3942 Gy, leading to a homogeneity index with a median of 0.8605. Those results can be explained by the fact that this real-time strategy delivers the dose to all regions of the tumor, but the way in which the choice between two positions is made is not optimal. This may be due to the fact that the choice between two positions does not consider the position of the Bragg peak. For example, during the first part of the treatment, when the Bragg peak occurs in the posterior region of the tumor, it is possible that the chosen position has a very low dose in the first layers of the tumor, thus strongly decreasing the sum, but a high dose at the back of the tumor where the Bragg peak occurs. However, the dose will still be delivered at the back of the tumor, increasing the dose at this level and thus the maximum. Therefore, the dose will not be delivered to the front of the tumor, where it was needed. One possible solution to this problem would be to implement more frequent energy changes. Another reason that could explain this heterogeneity within the tumor is that the choice is based on the dose in the voxels along the beam direction at single position and does not take into account the dose delivered in neighboring voxels.

In addition, we observe that this strategy is generally the one with the widest distribution interval. This means that it is not stable and the result varies greatly from one simulation to another. One of the possible reasons is that the minimum relies heavily on the previous accumulated dose, which relies on the noise in the beam. This noise varies from one simulation to the other, varying the way shots are fired, and changing the positions where the beams are shot.

The fourth strategy is **COGA**. We can see in Table 4.9 that the results obtained for the three COGA strategies are relatively similar even if it is true that the COGA_ONPODO strategy gives slightly worse results according to the dose homogeneity in the tumor, with a median equal to 0.6724 for this metric. This is probably due to the fact that this strategy calculates the gain of each position according to the delivered dose in the tumor depth along that position without taking into account neighboring voxels, and not according to the three-dimensions dose map like the two others COGA strategies (see 4.2.2-Characteristics of the different strategies).

Table 4.9: Values of the median of the different metrics obtained with the 3 COGA strategies and the ideal value of each obtained after 15 simulations.

	$D_{95\%}$ [Gy]	$D_{5\%}$ [Gy]	V_{2Gy} [%]	HI	D_{mean} in surr. OAR [Gy]	D_{mean} in ext. OAR [Gy]
COGA_ONPODO	1.4648	2.8294	71.6837	0.6724	1.0274	0.4335
COGA_TUVODO	1.5389	2.8211	71.297	0.6489	0.9921	0.5158
COGA_TUCO	1.5239	2.8211	71.9522	0.6389	0.9925	0.434
Ideal case	2	2	100	0	< 0.8	< 1.2

The COGA_TUVODO and COGA_TUCO strategies seem to be the most suitable to deliver a homogeneous dose within the tumor. As shown by the analysis of the different metrics, those strategies make it possible to strongly reduce the heterogeneity of the dose received in each tumor voxel. In those cases, the homogeneity index is around 0.64. This result was desired since they are implemented in such a way as to minimize the difference between the dose in each voxel.

In addition, we observe that, for each metric, the distribution intervals for the three COGA strategies are quite narrow, which means that they are stable. This stability can be explained by the fact that, when we look at the simulation, we see that the best positions to deliver the dose are very often identical at the beginning of the treatment. It is only after some time that a change in the firing pattern between the different simulations can be noted. In this case, the big difference with the FITWSACO strategy is that the COGA strategy evaluates the gain throughout the entire tumor, forcing a change of the beam position if the gain is minimum elsewhere, even if the constraints are still respected.

However, we also notice that the results are reversed for the surrounding OAR analysis since the mean delivered dose within this structure is the highest for those strategies. One potential reason for this finding is linked to safety margins. As already said, those strategies, unlike the previous three, use safety margins around the tumor to deliver the dose. This is reflected by the fact that the surrounding OAR is less spared than it was with the previous strategies. In addition, we also notice that the $V_{0.8Gy}$ increases with the three COGA strategies. This can be explained by the fact that they involve a radical change in the position of the Bragg peak at the halfway point of the treatment, i.e. when the mean delivered dose in the posterior region of the tumor is equal to 1 Gy. This leads to a dose delivered within the anterior part of the tumor for a certain period of time, meaning that the anterior area of the surrounding OAR is more reached, and thus increasing $V_{0.8Gy}$.

This in-depth analysis of each real-time strategy highlighted the formation of two groups within the 6 strategies. The first group is composed of the FIBESCMO, FITWSACO and MIACDO strategies, showing average results regarding the dose homogeneity within the tumor but fairly good results for the organs at risk. On the contrary, the three COGA strategies, belonging to the second group, deliver a homogeneous dose within the tumor but, on the other hand, require to relax the constraints on the neighbouring organs at risk.

4.3.3 Robustness of the best strategy

These different analyses highlight the advantages and shortcomings of each strategy. With these analyses, we can affirm that the three **COGA** strategies are the best, more specifically the COGA_TUCO one. As already said, this real-time strategy is inspired by the commonly used methods to optimise treatment plans using an objective function. However, instead of relying on theoretical results concerning the amount of dose delivered in one shot or the position of the tumor, our approach optimizes the dose delivery process in real-time. This is based on the actual values obtained at the time of the patient's treatment. In our approach, the algorithm continuously evaluates the optimal way to deliver the dose during the process without defining in advance a particular treatment plan.

Let's now focus on the robustness of the COGA_TUCO strategy. For that purpose, we will evaluate how the dose delivery behaves when some parameters of the simulation are modified. Only one parameter at a time will be changed.

First, we will analyze how the strategy adapts when changing the **size of the tumor**. As explained above, in this work we consider a 35 mm tumor. This corresponds to the average tumor size of a lung cancer. In this analysis, we will consider two cases: a 25 mm tumor and a 45 mm tumor. The 25 mm case represents a stage 1 cancer while the 45 mm tumor is relevant for a stage 2 cancer. In this case, we are going to look at how the homogeneity index evolves as the tumor size changes.

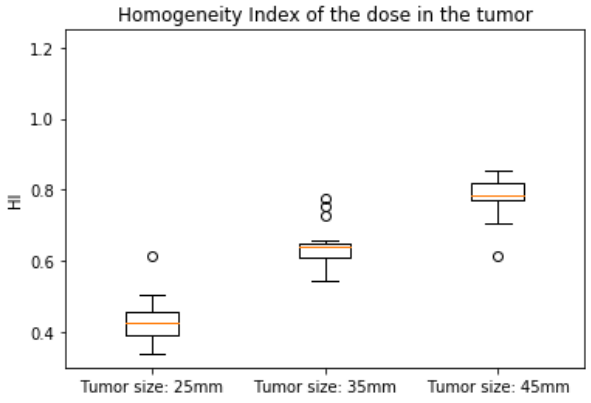

Figure 4.20: Boxplot of the homogeneity index for different tumor sizes. The orange line represents the median and the edges of the box indicate the 25th and 75th percentile. The circles show outliers.

As shown in Fig.4.20, the homogeneity index is greatly reduced for a small tumor, whereas it is higher for a bigger tumor. In the first case, it oscillates mainly between 0.35 and 0.5, while it is between 0.7 and 0.85 for a tumor of 45 mm. These observations can also be seen in Fig.4.21. Fig.4.21a shows that the $D_{5\%}$ within the small tumor is strongly reduced while the $D_{95\%}$ is increased, reducing the HI. On the other hand, Fig.4.21c shows that, for a large tumor, the $D_{5\%}$ is increased and $D_{95\%}$ is reduced, increasing the homogeneity index.

One possible reason for this observation is the control of the Bragg peak's position, which divides the length of the tumor along the beam direction into three identical segments. In the case of a smaller tumor, this induces that the three segments are too small, resulting in very frequent energy changes to ensure that the Bragg peak is correctly positioned for any anatomy, but without negatively affecting the way the dose is delivered. On the other hand, in the case of a larger tumor, this induces that the three segments are too large, resulting in no delivered dose at the back of the tumor. The central part of the tumor is therefore largely affected, implying that the homogeneity index increases. One improvement would be to consider the tumor size to determine the number of parts needed so that they keep the same size.

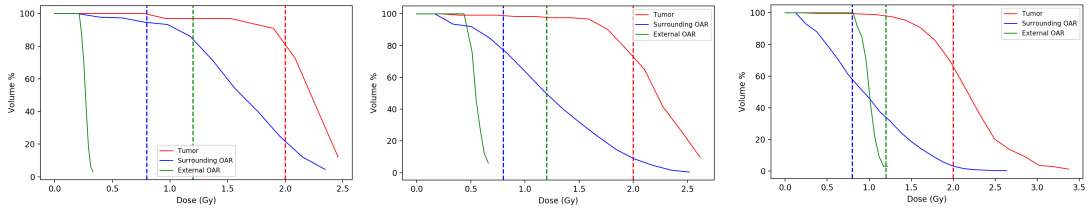

(a) Tumor size: 25 mm (b) Tumor size: 35 mm (c) Tumor size: 45 mm

Figure 4.21: Dose-Volume Histograms obtained with various tumor sizes: (a) 25mm, (b) 35mm and (c) 45 mm. In those figures, the red line represents the dose delivered within the tumor, the blue line within the surrounding OAR and the green line within the external OAR. The dotted lines show the constraints applied for each of these organs.

Moreover, as shown on Fig.4.21 with the blue lines, the size of the tumor also influences the delivered dose within the surrounding OAR. As shown in Fig.4.21c, the delivered dose within this organ decreases as the tumor size increases. In this case, the percentage of the surrounding OAR volume receiving the constraint dose is decreased compared to the case of a 35 mm tumor and is equal to 60%. On the contrary, the delivered dose within the surrounding OAR is increased for a smaller tumor. As shown on Fig.4.21a, more than 90% of this organ volume receives a dose greater than the constraint dose. This observation can be explained by the fact that the ratio between the tumor volume and the volume of the surrounding OAR is greatly reduced or increased as the tumor respectively increases or decreases in size.

This previous analysis led us to investigate the adaptation of the algorithm when the **size of the surrounding OAR** is modified. As mentioned above, the radius of this organ is initially set at twice the radius of the tumor, namely a size of 65 mm. This approximation will be modified here. We are going to look at what happens when the size of this organ is much larger than the size of the tumor. In reality, the lung is way bigger than twice the size of the tumor. Here we will consider a 85 mm lung. We did not consider this case earlier because a larger grid increases the computation time.

As shown on Fig.4.22a, a change in the size of the surrounding OAR has no effect on the homogeneity index of the delivered dose within the tumor. This one ranges mainly from 0.55 to 0.65 which are the same values than in the general case. On the other hand, we can observe on Fig.4.22b that the mean of the delivered dose within the surrounding OAR is strongly reduced for a surrounding OAR of 85 mm. In this case, the median is equal to 0.6386 Gy while it is equal to 0.9925 Gy in the general case. This means that the constraint on the surrounding OAR is always respected for this new size of 85 mm.

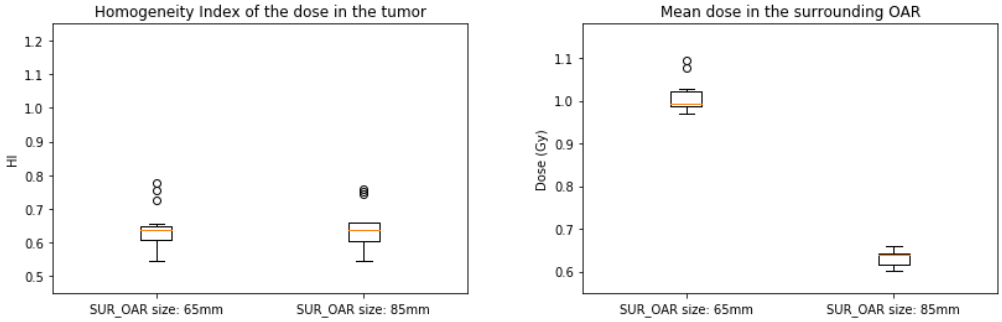

(a) Homogeneity Index

(b) Mean dose within the surrounding OAR

Figure 4.22: Boxplot of: (a) homogeneity index and (b) mean delivered dose within the surrounding OAR for different sizes of this organ. The orange line represents the median and the edges of the box indicate the 25th and 75th percentile. The circles show outliers.

This can also be observed on the DVHs obtained for two sizes of the surrounding OAR. The tumor curve in Fig.4.23a has a similar pattern than the one in Fig.4.23b, leading to an identical homogeneity index. On the contrary, the surrounding OAR curve is closer to the left in Fig.4.23b, meaning that the delivered dose within its entire volume is greatly reduced. This analysis shows that our approach is able to spare the surrounding OAR when it has a geometry closer to reality.

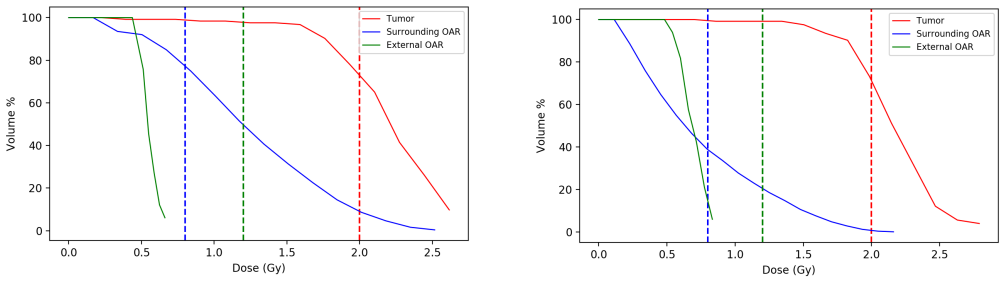

(a) Surrounding OAR size: 65 mm (b) Surrounding OAR size: 85 mm

Figure 4.23: Dose-Volume Histograms obtained with two surrounding OAR sizes: (a) 65mm, (b) 85mm. In those figures, the red line represents the dose delivered within the tumor, the blue line within the surrounding OAR and the green line within the external OAR. The dotted lines show the constraints applied for each of these organs.

Another important criterion to be studied is the **size of the external OAR**. In the general simulation, this organ is smaller than the tumor as it measures 25 mm. Here we will analyse how the algorithm behaves if we put a larger external OAR, measuring 35 mm. We will look to see if the dose constraint on this organ is still always satisfied when its size increases and if it is still possible to correctly reach the target in this case.

As shown in Fig.4.24a, the homogeneity index of the delivered dose within the target is slightly impacted when the size of the external OAR increases. Although it is always within the same range, it can be seen that the cases where the homogeneity index is greater than 0.7 are no longer outliers as it was the case with an external OAR of size 25 mm. This means that the HI is more frequently high. The median, which was equal to 0.6389 for a 25 mm external OAR, is equal to 0.6705 for an external OAR of size 35 mm. This slight increase can be explained by the fact that some regions of the tumor are less correctly reached by the beam since the external OAR is more in line with the beam.

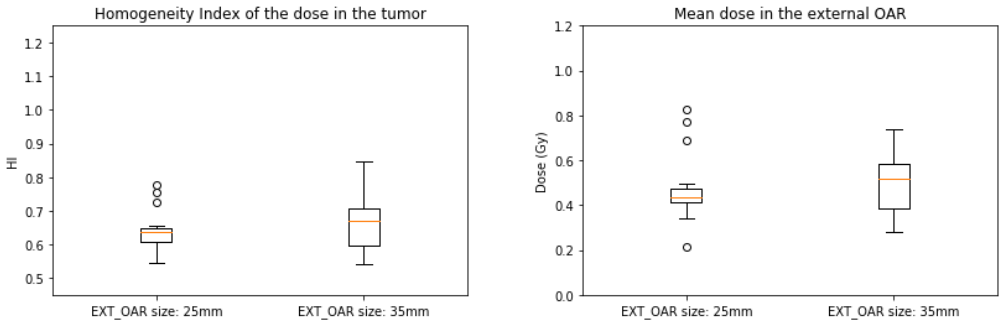

(a) Homogeneity Index (b) Mean dose within the external OAR

Figure 4.24: Boxplot of: (a) homogeneity index and (b) mean delivered dose within the external OAR for different sizes of this organ. The orange line represents the median and the edges of the box indicate the 25th and 75th percentile. The circles show outliers.

In addition, as shown in Fig.4.24b, the mean of the delivered dose within this organ is also slightly higher for a bigger external OAR. This means that this organ is more hit by the beam when its size increases, explaining the increase in the homogeneity index. Indeed, if the beam hits the external OAR, it delivers some dose in its volume, reducing its energy. If the beam energy is too strongly reduced, the Bragg peak will no longer occur at the desired location in the tumor and the dose will therefore not be delivered at the desired position. Despite the small increase in the mean of the delivered dose within its volume, the constraint on the dose remains respected in each simulation.

Those two observations can also be made with the help of the DVHs obtained in both cases. Fig.4.25a and Fig.4.25b display the DVH obtained with respectively an external OAR of size 25 mm and of 35 mm. In the case of an external OAR of size 35 mm, we can observe that the maximum delivered dose within the tumor is around 3 Gy and the minimum one is around 1.5 Gy. This implies that the homogeneity index is increased with respect to the one obtained in the case of an external OAR measuring 25 mm. Moreover, as shown in Fig.4.25b, the curve representing the delivered dose within the external OAR is more to the right than in Fig.4.25a, meaning that the mean of the delivered dose in this organ is increased.

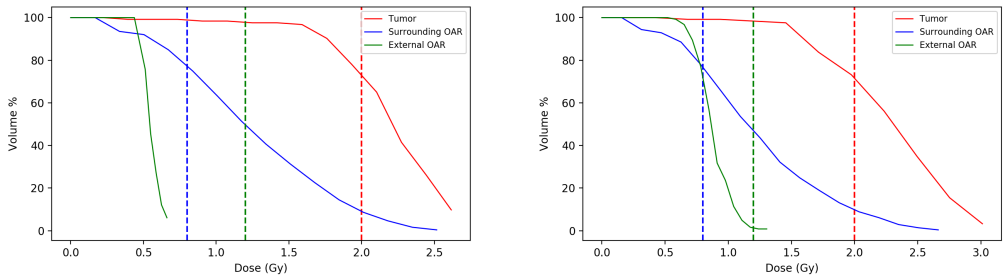

(a) External OAR size: 25 mm

(b) External OAR size: 35 mm

Figure 4.25: Dose-Volume Histograms obtained with two external OAR sizes: (a) 25mm, (b) 35mm. In those figures, the red line represents the dose delivered within the tumor, the blue line within the surrounding OAR and the green line within the external OAR. The dotted lines show the constraints applied for each of these organs.

Next, it is interesting to study how the dose distribution behaves when the quantity of the dose delivered in one shot varies. This factor is determined by the **monitor unit**. In this work, we set it at 10^9, which is a commonly used value. In this analysis, we will change the value of this parameter in order to analyse how the dose is delivered if it accumulates slower or, on the contrary, faster.

Fig.4.26 displays the homogeneity index of the delivered dose within the tumor for different values of the monitor unit: 10^8, 10^9 and 10^{10}. As shown in Fig.4.26, the homogeneity index is not significantly changed for a smaller value of the monitor unit. As displayed in the figure, the homogeneity index is still around 0.6 with a median equal to 0.6186. However, we can notice that the distribution interval is narrower, showing a stability of the strategy according to this metric when the monitor unit is equal to 10^8.

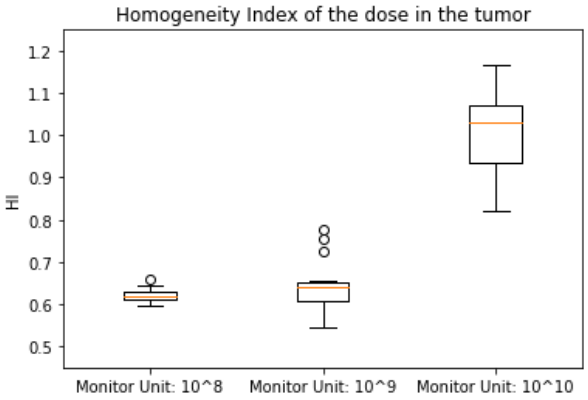

Figure 4.26: Boxplot of the homogeneity index for different monitor unit values. The orange line represents the median and the edges of the box indicate the 25th and 75th percentile. The circles show outliers.

On the other hand, as shown in Fig.4.26, the homogeneity index is greatly increased when the monitor unit is equal to 10^{10}. In this case the median is equal to 1.0296. This can be explained by the small difference between the prescribed dose and the delivered dose in one shot. Since the delivered dose in one shot is higher, only few shots are needed to deliver a higher dose than the prescribed one. Moreover, we notice that, in this case, the implemented energy change only occurs during a small part of the treatment. This may also explain the clear separation between the maximum and minimum dose as the Bragg peak occurs essentially in the same region of the tumor.

Fig.4.27 shows the DVHs obtained by running the simulation with the three monitor unit values. In this figure, it can be observed that the tumor curves in Fig.4.27a and Fig.4.27b are similar. In both cases, $D_{95\%}$ is around 1.5 Gy and $D_{5\%}$ around 2.5 Gy, indicating that the homogeneity index is close. On the other hand, the tumor curve in Fig.4.27c shows that the maximum delivered dose within this organ is above 3 Gy and the minimum one around 1.2 Gy, resulting in a higher homogeneity index.

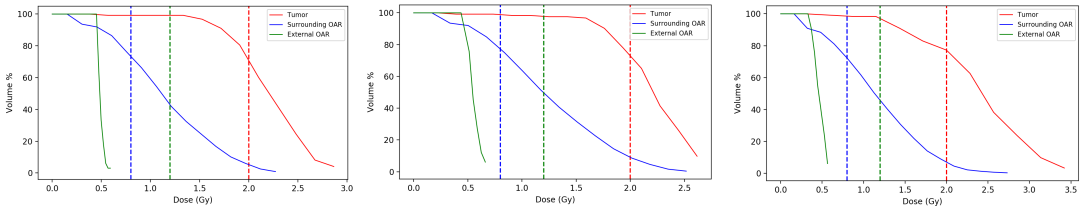

(a) Monitor unit: 10^8 (b) Monitor unit: 10^9 (c) Monitor unit: 10^{10}

Figure 4.27: Dose-Volume Histograms obtained with various values of the monitor unit: (a) 10^8, (b) 10^9 and (c) 10^{10}. In those figures, the red line represents the dose delivered within the tumor, the blue line within the surrounding OAR and the green line within the external OAR. The dotted lines show the constraints applied for each of these organs.

To close the analysis of the robustness of the best strategy, we perform a **multi-fractions treatment**. To have results as close to reality as possible, we will analyze how the dose is distributed after several sessions and if the results are still acceptable. To carry out this analysis, we consider the parameters summarized in Table 4.10.

Table 4.10: Parameters of the tumor, surrounding OAR and external OAR used for each fraction of the multi-fractions treatment simulation.

	Density [g/cm^3]	Diameter [mm]	Dose constraints [Gy]
Tumor	0.7	35	$D_{mean} = 2$
Surrounding OAR	0.5	85	$D_{mean} < 0.8$
External OAR	1.2	25	$D_{mean} < 1.2$

To perform this multi-fractions treatment, we simulate independent fractions and added the dose within each organ at the end of each fraction to obtain the final dose. Table 4.11 summarizes the results obtained for the various metrics as a function of the number of fractions simulated.

Table 4.11: Results obtained for multi-fractions treatments, depending on the number of fractions.

	$D_{95\%}$ [Gy]	$D_{5\%}$ [Gy]	V_{2Gy} [%]	HI	D_{mean} in surr. OAR [Gy]	D_{mean} in ext. OAR [Gy]
1 fraction	1.5598	2.8074	68.76	0.6238	0.6269	0.5839
1 fraction, ideal case	2	2	100	0	< 0.8	< 1.2
12 fractions	19.1111	32.3199	70.67	0.5504	7.8654	6.8531
12 fractions, ideal case	24	24	100	0	< 9.6	< 14.4
25 fractions	40.6871	67.7238	71.43	0.5407	16.3301	14.2015
25 fractions, ideal case	50	50	100	0	< 20	< 30

As shown in Table 4.11, the greater the number of fractions is, the better are the results. For example, the $D_{95\%}$ represents 81% of the prescribed dose in the 25-fractions treatment while it represents 77% of prescribed dose in the 1-fraction treatment. On the other hand, the value of the metric $D_{5\%}$ depicts 140% of the prescribed dose in the 1-fraction treatment and 135% in the 25-fractions treatment. This results in a decrease in the HI of the delivered dose within the tumor as the number of fractions increases. Moreover, these results also show that, whatever the number of fractions, the dose delivered to the two organs at risk does not exceed the dose imposed by the respective constraint.

Fig.4.28 shows the DVHs obtained for the 1-fraction, 12-fractions and 25-fractions treatments. These three figures highlight that the curves remain similar when the number of fractions increases.

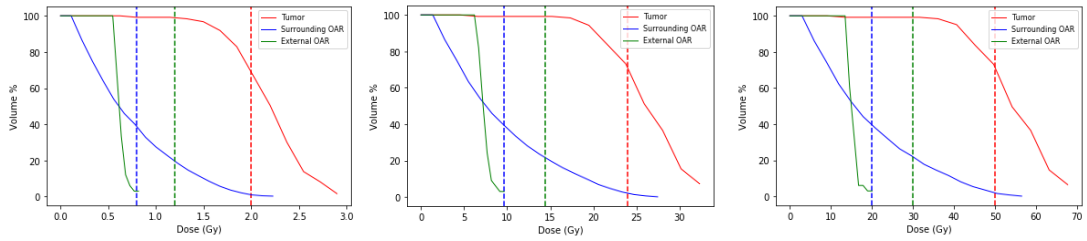

(a) 1-fraction treatment (b) 12-fractions treatment (c) 25-fractions treatment

Figure 4.28: Dose-Volume Histograms obtained with various values of fractions: (a) 1, (b) 12 and (c) 25. In those figures, the red line represents the dose delivered within the tumor, the blue line within the surrounding OAR and the green line within the external OAR. The dotted lines show the constraints applied for each of these organs.

4.4 Summary

In this chapter, we have seen the approach developed in this master thesis. We began by explaining how we created the anatomical structures and other parameters necessary to obtain a realistic approximation of the studied environment. Then, we developed the different strategies implemented for the real-time decision making approach. We compared the results given by each strategy using metrics that are commonly used to evaluate the quality of a DVH. Finally, we studied the robustness of the strategy that gave the best results. For that purpose, we varied some parameters to evaluate how the algorithm adapted to changes. A 25 mm tumor and a monitor unit of 10^8 gives a smaller homogeneity index of the delivered dose within the tumor. A small external OAR also decreases the homogeneity of the tumor dose and, in addition, decreases the frequency this organ is reached. A surrounding OAR of 85 mm shows that it is possible to meet the constraint on this organ when the ratio between the tumor volume and the surrounding OAR volume is reduced. Finally, we simulated a multi-fractions treatment to observe if the results of each independent fraction are correctly combined. This analysis highlighted that the dose within the tumor is more homogeneous for a greater number of fractions. Moreover, the constraints on the organs at risk are still respected regardless of the number of fractions.

Chapter 5

Conclusion

As we have seen in this work, radiotherapy is one of the three existing treatments for lung cancers. Proton therapy is a specific type of radiotherapy using protons. This technique, via the particularity of the Bragg peak, delivers the dose locally at the tumor level. Proton therapy uses the Pencil Beam Scanning to deliver the dose by scanning point by point the tumor volume. However, the use of this technique leads to the phenomenon of interplay when used with a mobile tumor. If the movements of the PBS and of the tumor are not synchronized, the delivered dose within the target is not uniform and the surrounding tissue is also irradiated.

Several methods have been studied to mitigate the effect of interplay. Some of those methods are used in routine while others are still in the research stage.

In this context, the objective of this work was to attempt to develop a new approach reducing the effect of interplay based on a real-time decision making. To carry out this project, we have exploited a maximum of the strengths of the techniques known to reduce the effect of interplay. The main feature of this work is the real-time decision making aspect. While the traditional clinical workflow in radiotherapy includes a treatment optimization phase in order to define the parameters of the machine needed to deliver the prescribed dose, our work defines those parameters in real-time when the patient is ready to receive the treatment. In this case, no treatment plan is defined before the dose delivery phase, allowing to take into account any unpredictable anatomical changes.

Our work then consisted of a numerical simulation that studies how the dose delivery takes place when the environment changes. For that purpose, we have defined various anatomical structures such as the tumor and surrounding organs at risk, but it was also necessary to design the protons beam or the respiratory motion to replicate the movement of the organs. Besides, to achieve this work, we have defined several real-time strategies. These strategies differ from one another in the way they select the optimal beam positions to deliver the dose in order to obtain a homogeneous dose within the target, while sparing surrounding organs at risk.

By using different metrics commonly employed to determine the quality of the treatment, we were able to compare the 6 real-time strategies we have implemented. This comparative analysis highlighted the separation of our strategies into two groups. On the one hand, the more traditional strategies and on the other hand, the innovative strategies specific to our approach. We saw that the strategies of the first group delivered a relatively

heterogeneous dose within the tumor, whereas it was more homogeneous when one of the strategies of the second group is used. However, we observed that it was necessary to slightly relax the constraints on the organs at risk in order to obtain a lower homogeneity index.

From there, we concluded that the strategies of the second group led to the best results. Therefore, we felt it was important to further develop the results we were achieving with the best strategy. For that purpose, we varied some key parameters of the simulation in order to evaluate how the algorithm adapted when they are modified. This analysis showed that the algorithm was robust to these parameter changes. In addition, this analysis highlighted that the algorithm worked better in certain configurations.

Now that we are at the end of this study, we realize that new perspectives can be explored. In the future, it could be interesting to change the value of the number of protons in the beam. A small value of this parameter causes noise in the dose delivery process, while a larger value causes a relatively uniform dose delivery around the desired position. In this work, we considered a beam composed of 50 protons. Then, it could be interesting to increase this value to see if the dose distribution within the tumor is more homogeneous. Moreover, another parameter that would be interesting to study in a future project is the size of the voxels. In this work, we considered a relatively small grid in order to speed up simulations and simplify the GUI while also considering the parameters commonly used in the treatment of lung cancer with proton therapy. This implies that the voxels used in this work are large. It would therefore be interesting to reduce their size in order to increase the number of voxels present in the grid and thus, increasing the number of possible positions in which the dose can be delivered. Furthermore, since each patient has a unique anatomy, it would be interesting to test our approach with different density values to evaluate whether it can correctly adapt the beam energy so that the dose is still delivered at the tumor level. An additional parameter that would be interesting to explore in a future study is the combination of various beam directions. In this work, we considered a fixed proton beam while, in reality, the beam direction changes during the treatment, making it possible to hit the tumor from different origins, leading to a more homogeneous delivered dose within the tumor and a lower mean dose within the external OAR. However, we would still need another year to improve our approach along these tracks.

Finally, we can conclude that the simulation of real-time decision making for dose delivery in proton therapy is obtaining promising results, which need to be improved in order to be clinically available. To this end, some tracks can be explored. With some enhancements, we hope that this approach can be used to improve the treatment of lung cancer and contribute to improve the quality of life of lung cancer patients.

Bibliography

[1] Futura Santé. *Cancer*. URL: https://www.futura-sciences.com/sante/definitions/medecine-cancer-108/. (accessed: 23.03.2020).

[2] WebMD. *Understanding Cancer - the basics*. URL: https://www.webmd.com/cancer/understanding-cancer-basics. (accessed: 23.03.2020).

[3] Fondation contre le cancer. *Le cancer en chiffres*. URL: https://www.cancer.be/le-cancer/le-cancer-en-chiffres. (accessed: 18.03.2019).

[4] Institut national du cancer. *Cancer du poumon:points-clés*. URL: https://www.e-cancer.fr/Patients-et-proches/Les-cancers/Cancer-du-poumon/Les-points-cles. (accessed: 23.03.2020).

[5] Fondation contre le cancer. *Cancer du poumon - Généralités*. URL: https://www.cancer.be/les-cancers/types-de-cancers/cancer-du-poumon. (accessed: 23.03.2020).

[6] ooreka. *Stades du cancer du poumon*. URL: https://cancer-du-poumon.ooreka.fr/comprendre/stades-cancer-poumon. (accessed: 23.03.2020).

[7] E. Sterpin K. Souris J. Lee G. Janssens A.M. Montero. "Engineering challenges in proton therapy". In: *Course 1: LGBIO2070* (2020).

[8] ooreka. *Chimiothérapie du cancer du poumon*. URL: https://cancer-du-poumon.ooreka.fr/comprendre/chimiotherapie-cancer-poumon. (accessed: 23.03.2020).

[9] eurekaSanté. *La radiothérapie dans le cancer du poumon*. URL: https://eurekasante.vidal.fr/maladies/cancers/cancer-poumon.html?pb=radiotherapie. (accessed: 23.03.2020).

[10] eurekaSanté. *La chirurgie du cancer du poumon*. URL: https://eurekasante.vidal.fr/maladies/cancers/cancer-poumon.html?pb=chirurgie. (accessed: 23.03.2020).

[11] J. Jonsson. "Integration of MRI into the radiotherapy workflow". In: *Umea University Medical Dissertations, Department of Radiation Sciences* (2013).

[12] American cancer society. *Getting External Beam Radiation Therapy*. URL: https://www.cancer.org/treatment/treatments-and-side-effects/treatment-types/radiation/external-beam-radiation-therapy.html. (accessed: 18.03.2020).

[13] C. M. Furdui. "Ionizing Radiation: Mechanisms and Therapeutics". In: *Antioxidants Redox Signaling* 21.2 (2014), pp. 218–220.

[14] A. Taylor M.E.B Powell. "Intensity-modulated radiotherapy - what is it?" In: *Cancer imaging* 4.2 (2004), pp. 68–73.

[15] Medical News Today. *Key concepts of radiobiology*. URL: http://edcan.org.au/edcan-learning-resources/supporting-resources/radiotherapy/radiobiology. (accessed: 07.04.2020).

[16] S. Breedveld D. Craft R. van Haveren B. Heijmen. "Multi-criteria optimization and decision-making in radiotherapy". In: *European Journal of Operational Research* 277 (2019), pp. 1–19.

[17] M. Rao D. Cao. *Comparison of anatomy-based, fluence-based and aperture-based treatment planning approaches for VMAT*. URL: https://www.researchgate.net/figure/DVH-comparison-for-a-lung-case-case-2-Thick-solid-lines-a-VMAT-thin-solid-lines_fig5_47500257. (accessed: 08.04.2020).

[18] M. Phillips E. Pedroni H. Blattmann T. Boehringer A. Coray S. Scheib. "Effects of respiratory motion on dose uniformity with charged particle scanning method". In: *Phys. Med. Biol* 37.1 (1992), pp. 223–234.

[19] Pyrexar Medical. *Bragg's peak*. URL: https://www.pyrexar.com/hyperthermia-blog. (accessed: 06.04.2020).

[20] Medical News Today. *Proton therapy as an option for treating cancer*. URL: https://www.medicalnewstoday.com/articles/268629. (accessed: 06.04.2020).

[21] B. Furlow. *Cost vs Benefits: The Controversy Over Proton Beam Radiotherapy*. URL: https://www.oncologynurseadvisor.com/home/cancer-types/general-oncology/cost-vs-benefits-the-controversy-over-proton-beam-radiotherapy/. (accessed: 19.05.2020).

[22] M. Vyfhuis N. Onyeuku T. Diwanji S. Mossahebi N. Amin S. Badiyan P. Mohindra C. Simone. "Advances in proton therapy in lung cancer". In: *Therapeutic Advances in Respiratory Disease* 12 (2018), pp. 1–16.

[23] C. Bert S. Grözinger E. Rietzel. "Quantification of interplay effects of scanned particle beams and moving targets". In: *Physics in Medicine and Biology* 53 (2008), pp. 2253–2265.

[24] R. Muirhead C. Featherstone A. Duffton K. Moore S. McNee. "The potential benefit of respiratory gated radiotherapy (RGRT) in non-small cell lung cancer". In: *Radiotherapy and Oncology* 95 (2010), pp. 172–177.

[25] J.F. Heron. *Radiothérapie du cancer*. URL: https://www.oncoprof.net/Generale2000/g08_Radiotherapie/g08_rt05.php. (accessed: 31.03.2020).

[26] Académie nationale de Médecine. *Le vocabulaire médical du XXIème siècle*. URL: http://dictionnaire.academie-medecine.fr/. (accessed: 31.03.2020).

[27] H. Li X.R. Zhu X. Zhang. "Reducing dose uncertainty for spot-scanning proton beam therapy of moving tumors by optimizing the spot delivery sequence". In: *International Journal of Radiation Oncology* 93.3 (2016), pp. 547–556.

[28] Xiaodong Zhang et al. "Evaluation and mitigation of the interplay effects for intensity modulated proton therapy for lung cancer in clinical setting". In: *Pract. Radiat. Oncology* (2015).

[29] A-C. Knopf A.J. Lomax. "In the context of radiosurgery - Pros and cons of rescanning as a solution for treating moving targets with scanned particle beams". In: *Physica Medica* 30 (2014), pp. 551–554.

[30] M. Riboldi R. Orecchia G. Baroni. "Real-time tumor tracking in particle therapy: technological developments and future perspectives". In: *The lancet: oncology* 13 (2012).

[31] D. De Ruysscher E. Sterpin K. Haustermans T. Depuydt. "Tumor movement in proton therapy: solutions and remaining questions: a review". In: *MDPI/Journal/-Cancers* 7 (2015), pp. 1143–1153.

[32] D. Winkel G. Bol P. Kroon B. van Asselen et al. "Adaptive radiotherapy: The Elekta Unity MR-linac concept". In: *Clinical and Translational Radiation Oncology* 18 (2019), pp. 54–59.

[33] C. Grassberger S. Dowdell A. Lomax G. Sharp J. Shackleford N. Choi H. Willers H. Paganetti. "Motion interplay as a function of patient parameters and spot size in spot scanning proton therapy for lung cancer". In: *International Journal of Radiation Oncology* 86.2 (2013), pp. 380–386.

[34] Y. Akino H. Wu R-J. Oh I. Das. "An effective method to reduce the interplay effects between respiratory motion and a uniform scanning proton beam irradiation for liver tumors: a case study". In: *Journal of Applied Clinical Medical Physics* 20.1 (2019), pp. 220–228.

[35] Wikipédia. *Simulation informatique*. URL: https://fr.wikipedia.org/wiki/Simulation_informatique. (accessed: 13.04.2020).

[36] Cancer.Net. *Lung cancer - Non-small cell : stages*. URL: https://www.cancer.net/cancer-types/lung-cancer-non-small-cell/stages. (accessed: 21.04.2020).

[37] J. C. Ye J. Chang Z. Li A. G. Wernicke. *Tumor Density, Size, and Histology in the Outcome of Stereotactic Body Radiation Therapy for Early-Stage Non–Small-Cell Lung Cancer: A Single-Institution Experience*. URL: https://www.cancernetwork.com/ars-2015/p097-tumor-density-size-and-histology-outcome-stereotactic-body-radiation-therapy-early-stage-non. (accessed: 22.05.2020).

[38] G. Noël D. Antoni I. Barillot B. Chauvet. "Delinéation des organes à risque et contraintes dosimétriques". In: *Cancer Radiothérapie* 20 (2016), pp. 36–60.

[39] J. Zeng R. Rengan. *Treating thoracic cancers with proton therapy: current practices, opportunities and challenges*. URL: https://iba-worldwide.com/sites/protontherapy/files/media_document/lung_white_paper_final_clean.pdf. (accessed: 15.05.2020).

[40] T. Kataria K. Sharma V. Subramani K.P. Karrthick S. S. Bisht. "Homogeneity Index: An objective tool for assessment of conformal radiation treatments". In: *J. Med. Phys* 37.4 (2012), pp. 207–213.

Appendix A

Selection of parameters

A.1 Spot sizes

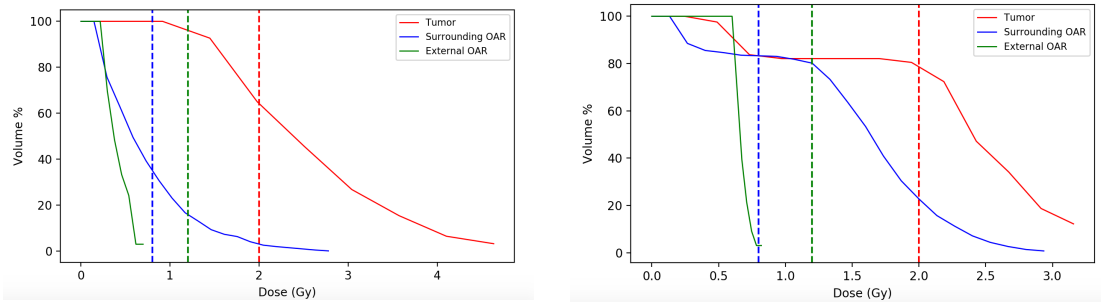

(a) DVH obtained with the small spot size

(b) DVH obtained with the big spot size

Figure A.1: This figure shows the DVHs obtained for the two extreme cases of spot size, small size ($\sigma_x = 1$, $\sigma_y = 1$) on the left and big size ($\sigma_x = 5$, $\sigma_y = 5$) on the right.

A.2 Number of simulations

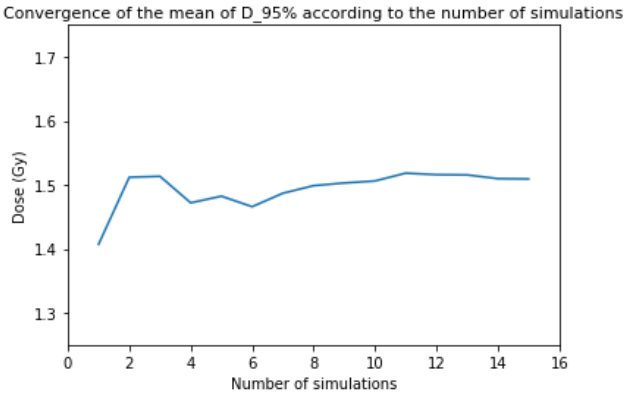

Figure A.2: Convergence of the mean of $D_{95\%}$ according to the number of simulations

UNIVERSITÉ CATHOLIQUE DE LOUVAIN
École polytechnique de Louvain
Rue Archimède, 1 bte L6.11.01, 1348 Louvain-la-Neuve, Belgique | **www.uclouvain.be/epl**